Star formation in galaxy mergers with realistic models of stellar feedback and the interstellar medium — Source link

Philip F. Hopkins, Thomas J. Cox, Lars Hernquist, Desika Narayanan ...+3 more authors

Institutions: University of California, Berkeley, Carnegie Learning, Harvard University, University of Arizona ...+3 more institutions

Topics: Star formation, Protogalaxy, Galaxy merger, Intergalactic star and Star cluster

Related papers:

- Stellar population synthesis at the resolution of 2003

- Gasdynamics and starbursts in major mergers

- Galactic stellar and substellar initial mass function

- Starburst99: Synthesis Models for Galaxies with Active Star Formation

- The Global Schmidt law in star forming galaxies

Share this paper:

Star formation in galaxy mergers with realistic models of stellar feedback and the interstellar medium

Philip F. Hopkins,[1][*] Thomas J. Cox,[2] Lars Hernquist,[3] Desika Narayanan,[4] Christopher C. Hayward[5] and Norman Murray[6,7]

[1]*Department of Astronomy, University of California Berkeley, Berkeley, CA 94720, USA*
[2]*Carnegie Observatories, 813 Santa Barbara Street, Pasadena, CA 91101, USA*
[3]*Harvard–Smithsonian Center for Astrophysics, 60 Garden Street, Cambridge, MA 02138, USA*
[4]*Steward Observatory, University of Arizona, 933 North Cherry Avenue, Tucson, AZ 85721, USA*
[5]*Heidelberger Institut für Theoretische Studien, Schloß-Wolfsbrunnenweg 35, D-69118 Heidelberg, Germany*
[6]*Canadian Institute for Theoretical Astrophysics, 60 St. George Street, University of Toronto, ON M5S 3H8, Canada*
[7]*Canada Research Chair in Astronomy and Astrophysics, Tier 2 - 2009-11-01, University of Alberta, Canada*

ABSTRACT

We use hydrodynamic simulations with detailed, explicit models for stellar feedback to study galaxy mergers. These high-resolution ($\sim$1 pc) simulations follow the formation and destruction of individual giant molecular clouds (GMC) and star clusters. We find that the final starburst is dominated by in situ star formation, fuelled by gas which flows inwards due to global torques. The resulting high gas density results in rapid star formation. The gas is self-gravitating, and forms massive ($\lesssim 10^{10}\,M_{\odot}$) GMC and subsequently super star clusters (with masses up to $10^8\,M_{\odot}$). However, in contrast to some recent simulations, the bulk of new stars which eventually form the central bulge are not born in super-clusters which then sink to the centre of the galaxy. This is because feedback efficiently disperses GMC after they turn several per cent of their mass into stars. In other words, most of the mass that reaches the nucleus does so in the form of gas. The Kennicutt–Schmidt law emerges naturally as a consequence of feedback balancing gravitational collapse, independent of the small-scale star formation microphysics. The same mechanisms that drive this relation in isolated galaxies, in particular radiation pressure from infrared photons, extend, with no fine-tuning, over seven decades in star formation rate (SFR) to regulate star formation in the most extreme starburst systems with densities $\gtrsim 10^4\,M_{\odot}\,\mathrm{pc}^{-2}$. This feedback also drives super-winds with large mass-loss rates; however, a significant fraction of the wind material falls back on to the discs at later times, leading to higher post-starburst SFRs in the presence of stellar feedback. This suggests that strong active galactic nucleus feedback may be required to explain the sharp cut-offs in SFR that are observed in post-merger galaxies.

We compare the results to those from simulations with no explicit resolution of GMC or feedback ['effective equation-of-state' (EOS) models]. We find that global galaxy properties are similar between EOS and resolved-feedback models. The relic structure and mass profile, and the total mass of stars formed in the nuclear starburst are quite similar, as is the morphological structure during and after mergers (tails, bridges, etc.). Disc survival in sufficiently gas rich mergers is similar in the two cases, and the new models follow the same scalings as derived for the efficiency of disc re-formation after a merger as derived from previous work with the simplified EOS models. While the global galaxy properties are similar between EOS and feedback models, subgalaxy-scale properties and the SFRs can be quite different: the more detailed models exhibit significantly higher star formation in tails and bridges (especially in

---

[*] E-mail: phopkins@astro.berkeley.edu

shocks), and allow us to resolve the formation of super star clusters. In the new models, the star formation is more strongly time-variable and drops more sharply between close passages. The instantaneous burst enhancement can be higher or lower, depending on the details of the orbit and initial structural properties of the galaxies; first-passage bursts are more sensitive to these details than those at the final coalescence.

1 INTRODUCTION

A wide range of observed phenomena indicate that gas-rich mergers are important to galaxy evolution and star formation. In the local Universe, the population of star-forming galaxies appears to transition from 'quiescent' (non-disturbed) discs [which dominate the *total* star formation rate (SFR)/infrared (IR) luminosity density] at the luminous IR galaxy (LIRG) threshold $10^{11}\,L_\odot$ ($\dot{M}_* \sim 10\text{--}20\,M_\odot\,\mathrm{yr}^{-1}$) to violently disturbed systems at a few times this luminosity. The most intense starbursts at $z = 0$, ultraluminous IR galaxies (ULIRGs; $L_{\mathrm{IR}} > 10^{12}\,L_\odot$), are invariably associated with mergers (e.g. Joseph & Wright 1985; Sanders & Mirabel 1996; Evans et al. 2010), and are fuelled by compact, central concentrations of gas (Scoville et al. 1986; Sargent et al. 1987) which provide material to feed black hole (BH) growth (Sanders et al. 1988), and to boost the concentration and central phase-space density of merging spirals to match those of ellipticals (Hernquist, Spergel & Heyl 1993; Robertson et al. 2006b). With central densities as large as ~1000 times those in Milky Way (MW) giant molecular clouds (GMC), these systems provide a laboratory for studying star formation under the most extreme conditions.

In addition, various studies have shown that the mass involved in these starburst events is critical for explaining the relations between spirals, mergers and ellipticals, and has a dramatic impact on the properties of merger remnants (e.g. Lake & Dressler 1986; Doyon et al. 1994; Shier & Fischer 1998; James et al. 1999; Genzel et al. 2001; Tacconi et al. 2002; Rothberg & Joseph 2004, 2006; Dasyra et al. 2006, 2007; Hopkins et al. 2009a,d). Even a small mass fraction of a few per cent formed in these nuclear starbursts can have dramatic implications for the mass profile structure (Mihos & Hernquist 1994a), phase-space densities (Hernquist et al. 1993), rotation and higher order kinematics (Cox et al. 2006b), kinematically decoupled components (Hoffman et al. 2009, 2010), stellar population gradients (Kewley et al. 2010; Soto & Martin 2010; Torrey et al. 2012a), and growth of the central BH (Di Matteo, Springel & Hernquist 2005; Hopkins et al. 2006; Hopkins & Hernquist 2009).

At higher redshifts ($z \sim 1\text{--}3$), galaxies with the luminosities of LIRGs and ULIRGs may be more 'normal' galaxies, in the sense that they are relatively undisturbed discs rather than mergers (Sajina et al. 2007; Yan et al. 2007; Dasyra et al. 2008; Dey et al. 2008; Melbourne et al. 2008). However, at those same redshifts, yet more luminous systems appear, including large populations of hyper-LIRGs ($L_{\mathrm{IR}} > 10^{13}\,L_\odot$) and bright submillimetre galaxies (e.g. Chapman et al. 2005; Younger et al. 2007, 2009b; Casey et al. 2009). These hyperluminous objects exhibit many of the traits associated with merger-driven starbursts, including morphological disturbances, and may be linked to the emergence of massive, quenched (non-star-forming), compact ellipticals at times as early as $z \sim 2\text{--}4$ (Papovich et al. 2005; Tacconi et al. 2006; Schinnerer et al. 2008; Tacconi et al. 2008; Younger et al. 2008b; Chapman et al. 2009). Reproducing their abundance and luminosities remains a challenge for current models of galaxy formation (Baugh et al. 2005; Swinbank et al. 2008; Younger et al. 2009a; Hayward et al. 2010, 2011; Narayanan et al. 2010).

Modelling the consequences of these mergers for star formation and the nuclear structure of galaxies requires following the highly non-linear, resonant and chaotic interplay between gas (with shocks, cooling, star formation and feedback), stars and dark matter over a very large dynamic range. High-resolution numerical hydrodynamic simulations are the method of choice. However, until recently, computational limitations have made it impossible to resolve the ~pc (and <1000 yr) scales of structure in the interstellar medium (ISM) relevant for star formation and stellar feedback while following the four or five orders of magnitude larger global evolution of a galaxy or merger. Perforce, most previous models have adopted a variety of subgrid approaches to describe 'effective' ISM properties below the resolution scales of the simulations.

All numerical galaxy simulations require some sort of 'subgrid' model; for example, even with box sizes of the order of 1 pc, current star formation simulations treat radiative feedback in a very approximate manner, while it is clear that such feedback is crucial to determining, for example, the initial mass function (IMF). Unfortunately, without a physically well founded subgrid model, the predictive power of numerical simulations is limited. If the average star formation properties are put in by hand (and they are in most galaxy-scale simulations to date), the global SFR clearly cannot be predicted. Similarly, if the effects of stellar feedback are put in by hand, e.g. by invoking an 'effective pressure' or turbulent dispersion, in order to suppress runaway cooling and clumping, the detailed physics and implications for star formation cannot be determined. Moreover, it is by no means clear if commonly used prescriptions capture the key physics, nor whether they can be extrapolated from 'quiescent' systems (which are typically used to calibrate the models) to the very different ISM conditions in mergers. Typically, subgrid models also have several adjustable parameters, which further limit their predictive power; it is often unclear whether observational constraints imply differences in the merger dynamics or more subtle tweaks in the subgrid ISM assumptions. This has occasionally led to contradictory conclusions in the literature.

Numerical simulations of isolated galaxies and galaxy mergers can now achieve the dynamic range required to resolve the formation of GMC and ISM structure, ~1–10 pc (see e.g. Saitoh et al. 2008; Tasker & Tan 2009; Bournaud et al. 2010; Dobbs, Burkert & Pringle 2011). However, improving resolution alone – beyond the implicit 'averaging' scales for the ISM model – has no clear meaning if the physics that govern star formation and ISM structure on these scales are not included. Generally, models have not attempted to include these physics or have included a very limited subset of the relevant processes. In fact, a large number of feedback mechanisms may drive turbulence in the ISM and help disrupt GMC, including: photoionization, stellar winds, radiation pressure from ultraviolet (UV) and IR photons, protostellar jets, cosmic rays, supernovae

(SNe), and gravitational cascades from large scales (e.g. Mac Low & Klessen 2004, and references therein).

In Hopkins, Quataert & Murray (2011, hereafter Paper I) and Hopkins, Quataert & Murray (2012a, hereafter Paper II), we developed a new set of numerical models to incorporate feedback on small scales in GMC and star-forming regions into simulations with pc-scale resolution.[1] These simulations include the momentum imparted locally (on sub-GMC scales) from stellar radiation pressure, radiation pressure on larger scales via the light that escapes star-forming regions, H II photoionization heating, as well as the heating, momentum deposition and mass loss by SNe (Type I and Type II) and stellar winds [from O and asymptotic giant branch (AGB) stars]. The feedback is tied to the young stars, with the energetics and time dependence taken directly from stellar evolution models. Our method also includes cooling to temperatures $<$ 100 K, and a treatment of the molecular/atomic transition in gas and its effect on star formation.

We showed in Papers I and II that in isolated disc galaxies these feedback mechanisms produce a quasi-steady ISM in which GMC form and disperse rapidly, after turning just a few per cent of their mass into stars. This leads to an ISM with phase structure, turbulent velocity dispersions, scaleheights and GMC properties (mass functions, sizes, scaling laws) in reasonable agreement with observations. In Hopkins, Quataert & Murray (2012b, hereafter Paper III), we showed that these same models of stellar feedback *predict* the elusive winds invoked in almost all galaxy formation models; the *combination* of multiple feedback mechanisms is critical to give rise to massive, multiphase winds having a broad distribution of velocities, with material both stirred in local fountains and unbound from the disc.

Papers I and II showed that the global SFR found in the simulations did not depend on the subgrid model for star formation, over a broad range of subgrid model parameters and even model types. The conclusion drawn was that the rate of star formation in the simulations was controlled by the amount of feedback required to maintain the gas disc in hydrostatic equilibrium, and with a Toomre Q parameter of the order of unity. If this is true in real galaxies, it will simplify the task of understanding galaxy formation greatly.

In this paper, we extend these models to idealized major mergers between galaxies. In this first exploration, we compare some of the global properties of the remnants – particularly those tied to star formation and ISM physics – to the results of simulations using more simplified subgrid ISM/feedback models. Specifically, we investigate the consequences of a more detailed and explicit treatment of the ISM for the star formation histories, spatial distribution of stellar mass and starburst stars, survival and re-formation of gas discs, and origins of the global Kennicutt–Schmidt (KS) law. All these properties can be compared to the results from previous subgrid models in a straightforward manner. We also test the proposition that the SFR is controlled by feedback, in mergers as well as in quiescent galaxies, since we do not adjust our star formation prescription.

In companion papers, we examine in more detail some of the phenomena that could not be predicted with previous models: the phase structure of the ISM and properties of starburst 'super-winds' driven by stellar feedback, as well as the physics of star cluster formation in tidally shocked and starburst regions.

---

[1] Movies of these simulations are available at https://www.cfa.harvard.edu/ ~phopkins/Site/Movies_sbw_mgr.html

2 METHODS

The simulation techniques and galaxy models used here are described in detail in Paper I (section 2 and tables 1– 3) and Paper II (section 2). We briefly summarize the most important properties here. The simulations were performed with the parallel TreeSPH code GADGET-3 (Springel 2005), in its fully conservative formulation (Springel & Hernquist 2002). They include stars, dark matter and gas, with cooling, shocks, star formation and stellar feedback.

2.1 Disc models

We implement the ISM prescription in four distinct initial disc models spanning a range of galaxy types (summarized in Table 1). Each has a bulge, stellar and gaseous disc, halo, and central BH (although to isolate the role of stellar feedback, models for BH growth and feedback are disabled). At our standard resolution, each model has $\approx(0.3–1) \times 10^8$ total particles, giving particle masses of 500– $1000 \, \mathrm{M}_\odot$ and 1–5 pc smoothing lengths. A couple of ultrahigh-resolution runs (of isolated versions of these discs) for convergence tests employ $\approx 10^9$ particles with sub-pc resolution.[2] The disc models include:

(1) *SMC.* A Small Magellanic Cloud (SMC) like dwarf, with baryonic mass $M_{\mathrm{bar}} = 8.9 \times 10^8 \, \mathrm{M}_\odot$ and halo mass $M_{\mathrm{halo}} = 2 \times 10^{10} \, \mathrm{M}_\odot$ (concentration $c = 15$), a Hernquist (1990) profile bulge with a mass $m_{\mathrm{b}} = 10^7 \, \mathrm{M}_\odot$, and exponential stellar ($m_{\mathrm{d}} = 1.3 \times 10^8 \, \mathrm{M}_\odot$) and gas discs ($m_{\mathrm{g}} = 7.5 \times 10^8 \, \mathrm{M}_\odot$) with scalelengths $h_{\mathrm{d}} = 0.7$ and $h_{\mathrm{g}} = 2.1$ kpc, respectively. The initial stellar scaleheight is $z_0 = 140$ pc and the stellar disc is initialized such that the Toomre $Q = 1$ everywhere. The gas and stars are initialized with uniform metallicity $Z = 0.1 \, Z_\odot$.

(2) *MW.* A MW-like galaxy, with halo and baryonic properties of $(M_{\mathrm{halo}}, c) = (1.6 \times 10^{12} \, \mathrm{M}_\odot, 12)$ and $(M_{\mathrm{bar}}, m_{\mathrm{b}}, m_{\mathrm{d}}, m_{\mathrm{g}}) = (7.1, 1.5, 4.7, 0.9) \times 10^{10} \, \mathrm{M}_\odot$, $Z = Z_\odot$ and scalelengths $(h_{\mathrm{d}}, h_{\mathrm{g}}, z_0) = (3.0, 6.0, 0.3)$ kpc.

(3) *Sbc.* An LIRG-like galaxy (i.e. a more gas rich spiral than is characteristic of those observed at low redshifts) with $(M_{\mathrm{halo}}, c) = (1.5 \times 10^{11} \, \mathrm{M}_\odot, 11)$, $(M_{\mathrm{bar}}, m_{\mathrm{b}}, m_{\mathrm{d}}, m_{\mathrm{g}}) = (10.5, 1.0, 4.0, 5.5) \times 10^9 \, \mathrm{M}_\odot$, $Z = 0.3 \, Z_\odot$ and $(h_{\mathrm{d}}, h_{\mathrm{g}}, z_0) = (1.3, 2.6, 0.13)$ kpc.

(4) *HiZ.* A high-redshift massive starburst disc, chosen to match the properties of the observed non-merging but rapidly star forming SMG population, with $(M_{\mathrm{halo}}, c) = (1.4 \times 10^{12} \, \mathrm{M}_\odot, 3.5)$ and a virial radius appropriately rescaled for a halo at $z = 2$ rather than $z = 0$, $(M_{\mathrm{bar}}, m_{\mathrm{b}}, m_{\mathrm{d}}, m_{\mathrm{g}}) = (10.7, 0.7, 3, 7) \times 10^{10} \, \mathrm{M}_\odot$, $Z = 0.5 \, Z_\odot$ and $(h_{\mathrm{d}}, h_{\mathrm{g}}, z_0) = (1.6, 3.2, 0.32)$ kpc.

2.2 Merger parameters

The purpose of this paper is to contrast models with and without explicit stellar feedback, not to present a systematic study of all merger parameters – extensive studies of this nature can be found in the literature (Barnes & Hernquist 1992; Naab, Burkert & Hernquist 1999; Barnes 2002; Cox et al. 2006b, 2008; Robertson et al. 2006b; di Matteo et al. 2007; Burkert et al. 2008; Younger et al. 2008a;

---

[2] These tests are described in Paper I and Paper II, and used to check convergence in small-scale ISM properties. We have also run every simulation described in this paper with 10 times fewer particles (two times larger softening); although the small-scale properties such as the structure of individual star clusters differ, all properties plotted in this paper (more global values in general) are found to be indistinguishable.

Table 1. Galaxy models.

Model	ϵ_g (pc)	M_{halo} (M$_\odot$)	c	V_{max} (km s^{-1})	M_{bary} (M$_\odot$)	M_b (M$_\odot$)	a (kpc)	M_d (M$_\odot$)	r_d (kpc)	h (pc)	M_g (M$_\odot$)	r_g (kpc)	f_{gas}	Z (Z$_\odot$)
SMC	1.0	2.0e10	15	46	8.9e8	1e7	0.25	1.3e8	0.7	140	7.5e8	2.1	0.56	0.1
Sbc	3.1	1.5e11	11	86	1.05e10	1e9	0.35	4e9	1.3	320	5.5e9	2.6	0.36	0.3
MW	4.0	1.6e12	12	190	7.13e10	1.5e10	1.0	4.73e10	3.0	300	0.9e10	6.0	0.09	1.0
HiZ	7.0	1.4e12	3.5	230	1.07e11	7e9	1.2	3e10	1.6	130	7e10	3.2	0.49	0.5

Parameters describing our (isolated) galaxy models, used as the initial conditions for all of the mergers:
(1) model name: shorthand for models of an isolated SMC-mass dwarf (SMC); local gas-rich galaxy (Sbc); MW analogue (MW); and high-redshift massive starburst (HiZ). (2) ϵ_g: gravitational force softening. Higher resolution tests of the isolated galaxies use half this value (Paper I). (3) M_{halo}: halo mass. (4) c: halo concentration. Values lie on the halo mass–concentration relation at each redshift ($z = 0$ for SMC, Sbc and MW; $z = 2$ for HiZ). (5) V_{max}: halo maximum circular velocity. (6) M_{bary}: total baryonic mass. (7) M_b: bulge mass. (8) a: Hernquist (1990) profile scalelength for the bulge. (9) M_d: stellar disc mass. (10) r_d: stellar disc scalelength. (11) h: stellar disc scaleheight. (12) M_g: gas disc mass. (13) r_g: gas disc scalelength (gas scaleheight determined so that $Q = 1$). (14) f_{gas}: average gas fraction of the disc inside the stellar R_e $[M_g[<R_e]/(M_g[<R_e] + M_d[<R_e]]$. The total gas fraction, including the extended disc, is $\sim$50 per cent larger. (15) Z: initial metallicity (in solar units) of the gas and stars.

Hoffman et al. 2009; Jesseit et al. 2009). We therefore focus on a small but representative subset of possible mergers.

We consider equal-mass mergers [merging identical copies of galaxies (1)–(4)]. The pairs are placed on parabolic orbits (motivated by cosmological simulations; see Benson 2005; Khochfar & Burkert 2006) with the spin axis of each disc specified by θ and ϕ in spherical coordinates. We choose two representative orientations from among those which have been studied in a number of other works (Barnes 1988; Hernquist 1992, 1993; Naab & Burkert 2003; Cox et al. 2006b). The first (orbit *e* in Cox et al. 2006b) is near-prograde with $(\theta_1, \phi_1, \theta_2, \phi_2) = (30, 60, -30, 45)$; the second (orbit *f*) is near-retrograde (or polar-retrograde) with $(\theta_1, \phi_1, \theta_2, \phi_2) = (60, 60, 150, 0)$. This spans both a strong resonant interaction (prograde) and a weak, out-of-resonance (retrograde) interaction. We choose these rather than perfectly prograde $(\theta_1, \phi_1, \theta_2, \phi_2) = (0, 0, 0, 0)$ and retrograde $(\theta_1, \phi_1, \theta_2, \phi_2) = (180, 0, 180, 0)$ orbits because there are known pathological behaviours associated with the narrow phase space of perfectly resonant orbits.

We have compared a subset of low-resolution simulations that vary orbital inclinations and pericentric passage distances; the variation in remnant properties is consistent with previous studies (e.g. Cox et al. 2006b). However, this variation is largely a dependence on the strength of gravitational torques and total angular momentum; the *differences* between models with/without feedback do not dramatically depend on these properties. In any case, our *e* and *f* orbits reasonably bracket the range from most to least violent orbits.

2.3 Explicit feedback models

The most important physics in these simulations is the model of stellar feedback. We include feedback from a variety of mechanisms, each of which we briefly describe below. More details about our implementations of this physics are given in Paper I and Paper II. We use a Kroupa (2002) IMF throughout and use STARBURST99 (Leitherer et al. 1999) to calculate the stellar luminosity, mass return from stellar winds, supernova rate, etc., as a function of the age and metallicity of each star particle.

(1) *Local momentum deposition from radiation pressure, SNe and stellar winds*. In Paper I, we present the radiation pressure aspect of this model for feedback from young star clusters in detail. At each time-step, gas particles identify the nearest density peak representing the centre of the nearest star-forming 'clump' or GMC

analogue. We calculate the total luminosity of the star particles inside the sphere defined by the distance from the centre of this star-forming region to the gas particle of interest; the incident flux on the gas is then determined assuming that the local star-forming region is optically thick to the UV radiation.

The rate of momentum deposition from radiation pressure is then $\dot{P}_{rad} \approx (1 + \tau_{IR}) L_{incident}/c$, where the term $1 + \tau_{IR}$ accounts for the fact that most of the initial optical/UV radiation is absorbed and re-radiated in the IR; $\tau_{IR} = \Sigma_{gas} \kappa_{IR}$ is the optical depth in the IR, which allows for the fact that the momentum is boosted by multiple scatterings in optically-thick regions. Here Σ_{gas} is calculated self-consistently as the average surface density of the identified clump, with $\kappa_{IR} \approx 5 (Z/Z_\odot) \, g^{-1} \, cm^2$ approximately constant over the relevant physical range of dust temperatures. The imparted acceleration is directed along the flux vector. In Paper I, we discuss numerous technical aspects of this implementation – such as the effects of resolution, photon leakage, and how the momentum is discretized – and show that essentially all our conclusions are robust to uncertainties in these choices.

The *direct* momentum of SN ejecta and stellar winds, $\dot{P}_{SNe}$ and $\dot{P}_w$, respectively, is similarly tabulated from STARBURST99 and injected as an appropriate function of age and metallicity to the gas within a smoothing length of each star. This source of turbulent energy is almost always smaller than that due to radiation pressure discussed above. In some cases, however, in particular in dwarf galaxies, the work done by bubbles of gas shock-*heated* by SNe and/or stellar winds is dynamically important; this is discussed below.

(2) *Supernova and stellar wind shock heating*. The gas shocked by SNe and stellar winds can be heated to high temperatures, generating bubbles and filaments of hot gas. We tabulate the Type I and Type II SN rates from Mannucci, Della Valle & Panagia (2006) and STARBURST99, respectively, as a function of age and metallicity for all star particles, and stochastically determine at each time-step if a SN occurs. The SNe are resolved discretely in time (as opposed to continuous energy injection). For each SN, the appropriate thermal energy is injected into the gas within a smoothing length of the star particle. Similarly, stellar winds are assumed to shock locally and so we inject the appropriate tabulated mechanical power $L(t, Z)$ as a continuous function of age and metallicity into the gas within a smoothing length of the star particles. The specific energy of these stellar winds is large for young stellar populations in which fast winds from massive stars dominate, but declines rapidly at later times when slower, AGB winds dominate.

(3) *Gas recycling.* Gas mass is returned continuously to the ISM from stellar evolution, at a rate tabulated from SNe and stellar mass loss in STARBURST99. The integrated mass fraction recycled is ~ 0.3.

(4) *Photoheating of H II regions.* For each star particle, we tabulate the rate of production of ionizing photons; starting from the nearest gas particle and moving radially outwards, we then ionize each non-ionized gas particle (using the gas and stellar properties to determine the photon production rate needed to maintain the particle as fully ionized). Gas which is ionized is immediately heated to $\sim 10^4$ K, unless is already above this temperature; moreover, the gas is not allowed to cool below 10^4 K until it is no longer in an H II region. This method allows for overlapping, non-spherical H II regions that can extend to radii $\sim$ kpc.

(5) *Long-range radiation pressure.* Radiation pressure from photons absorbed in the immediate vicinity of stars is captured in mechanism (1). However, photons that escape these regions can still be absorbed at larger radii. For each star particle, we construct the intrinsic spectral energy distribution (SED) (L_ν) as a function of age and metallicity; we then use the local density and density gradients to estimate the integrated column density and attenuation of the SED using $\tau_\nu = \kappa_\nu \Sigma \approx \kappa_\nu \rho \, (h_{\rm sml} + |\nabla \ln \rho|^{-1})$, where $h_{\rm sml}$ is the smoothing length and κ_ν is the frequency-dependent opacity [assuming dust opacities that scale with metallicity, as in equation (1) above]. The resulting 'escaped' SED gives a frequency-dependent flux $\boldsymbol{F}_\nu$ that is propagated to large distances. We construct a force tree for this long range force in an identical fashion to the gravity tree, since after attenuating the flux near the star particle, the stellar flux is assumed to decrease $\propto r^{-2}$. Each gas particle then sees an incident net flux vector $\boldsymbol{F}_\nu^i$, integrated over all stars in the galaxy.

Extensive numerical tests of the feedback models are presented in Paper I, Paper II and Paper III.

In these models, gas follows an atomic cooling curve with additional fine-structure cooling to <100 K, with no cooling floor imposed. Star formation follows the model in Hopkins, Quataert & Murray (in preparation). Regions that are locally self-gravitating on the smallest resolved scale, i.e. which have $\alpha \equiv \delta v^2 \, \delta r / G \, m_{\rm gas}(< \delta r) \rightarrow (|\nabla \cdot \boldsymbol{v}|^2 + |\nabla \times \boldsymbol{v}|^2)/(2 \, G \rho) < 1$, should collapse to much higher densities in a free-fall time absent feedback; we therefore assign them an instantaneous SFR of $\dot{\rho}_* = \rho/t_{\rm ff}(\rho)$. We stress that because feedback is present and can regulate against further collapse once stars form, the average efficiency in the dense gas is much lower (typically ~ 1 per cent). We further follow Krumholz & Gnedin (2011) and calculate the molecular fraction within the dense gas as a function of the local column density and metallicity, and allow star formation only from that gas; however, as shown in Paper II and Hopkins et al. (in preparation) this has essentially no effect on our results.

As noted in the Introduction, we showed in Paper I and Paper II that the galaxy structure and SFR are basically independent of the small-scale star formation law, density threshold (provided it is high), and treatment of molecular chemistry, because the structure and SFR are feedback-regulated. As a further test of this result, we have re-run several of the models described here with the more simplified (and frequently used) star formation prescription in which star formation is restricted to occur only in gas above a density $n > 1000 \, {\rm cm}^{-3}$, with a rate $\dot{\rho}_* = 0.015 \rho/t_{\rm ff}$ corresponding to observed average efficiencies 'enforced'. This has almost no effect on global properties or the galaxy-average SFRs, but it does tend to 'smear out' the SFR in dense regions such as the merging nuclei, where *all* the gas is well above this threshold.

2.4 Models with an 'effective' equation of state

In previous work on galaxy mergers, it was not possible to explicitly resolve the processes described above. Instead, simulations used a variety of subgrid approaches to model some 'effective' ISM properties on the resolution scales of the simulations (often a few hundred pc).

We want to assess the accuracy of such subgrid models. We therefore compare otherwise identical disc merger models using the effective equation-of-state (EOS) approach in Springel & Hernquist (2003). Since high-density GMC are not resolved, the star formation threshold is lower, chosen to represent densities where multiphase structure should appear (here we adopt $n > 1 \, {\rm cm}^{-3}$); the efficiency must be correspondingly tuned to match the global Kennicutt relation (here $\dot{\rho}_* = 0.03 \, \rho/t_{\rm ff}$). The model attempts to account for the complex subgrid feedback physics described above by simply assigning the star-forming gas an effective sound speed $c_{\rm eff}$ representing, for example, a subgrid turbulent ISM pressure.

In the model of Springel & Hernquist (2003), the effective pressure is motivated by the ISM model in McKee & Ostriker (1977). Because the assumed subgrid ISM properties are uncertain, the model allows for interpolation in the EOS with the parameter $q_{\rm eos}$ (see Springel, Di Matteo & Hernquist 2005; Springel & Hernquist 2005; Robertson et al. 2006a,c). The standard 'maximal feedback' case ($q_{\rm eos} = 1$) assumes 100 per cent of the energy from SN couples to an intercloud diffuse phase with long cooling times; this leads to a fairly 'stiff' EOS, $c_{\rm eff} \sim 50$–$200 \, {\rm km \, s}^{-1}$. The opposite 'weak-feedback' case ($q_{\rm eos} = 0$) has $c_{\rm eff} \sim 10 \, {\rm km \, s}^{-1}$, motivated by the minimum dispersion observed in gas in most galaxies. This is quite similar to the effective EOS used in Teyssier, Chapon & Bournaud (2010). Intermediate values interpolate as $c_{\rm eff}^2 = q_{\rm eos} \, c_{\rm eff}^2[q = 1] + (1 - q_{\rm eos}) \, c_{\rm eff}^2[q = 0]$. In Hopkins & Quataert (2010), various choices are compared to observations of star-forming systems as a function of density; they suggest that $q_{\rm eos} \sim 0.1$–0.3 gives a reasonable representation of the observations. We therefore adopt $q_{\rm eos} = 0.25$ as our standard choice; however, we have also re-run comparison models with $q_{\rm eos} = 1$ and our conclusions are nearly identical.

3 MORPHOLOGIES

3.1 Merger morphologies

Figs 1 and 2 show the gas and stars in some representative stages of the merger simulations, for our standard case ('explicit' feedback model) where all feedback mechanisms are present. Figs 4 and 5 and Figs A1–A4 extend this to show the gas and stars in a number of merger stages, from different viewing angles, for each merger. Fig. 5 specifically compares this in a simulation with the explicit feedback model and one with identical initial conditions using the subgrid treatment of the ISM and star formation.

In each image set, the gas maps show the projected gas density (intensity) and temperature (colour: with blue representing the cold molecular gas at $T \lesssim 1000$ K, pink representing the warm ionized gas at $\sim 10^4$–10^5 K, and yellow representing the hot, X-ray-emitting gas at $\gtrsim 10^6$ K).[3] The stellar maps show a mock three-colour

---

[3] The projected temperatures are logarithmically averaged and surface density weighted, so reflect the temperature of most of the line-of-sight gas mass, rather than the temperature that contains most of the thermal energy.
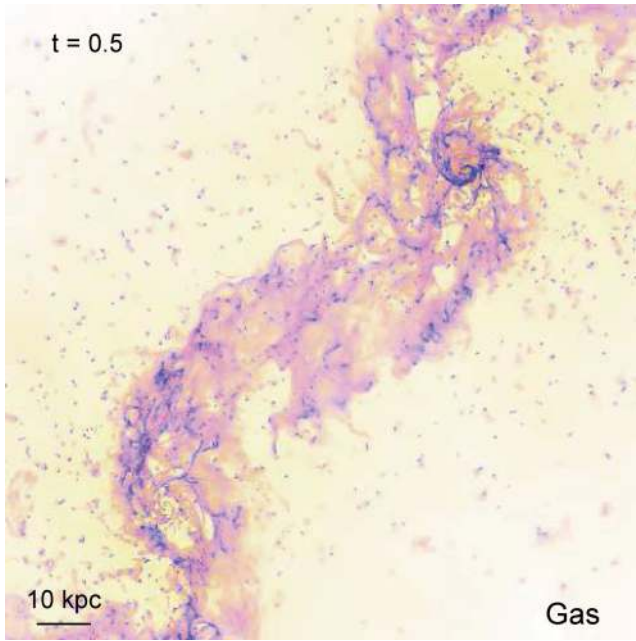
Figure 1. Morphology of the gas in a standard simulation (high resolution with all explicit feedback mechanisms included) of a merger of the HiZ disc model: a massive, $z \sim 2$–4 starburst disc merger. The time is near apocentre after the first passage. This colour projection emphasizes the cold, star-forming gas. Brightness encodes projected gas density (light to dark with increasing density; logarithmically scaled with an $\approx$4 dex stretch); colour encodes gas temperature with the blue/violet material being $T \lesssim 1000$ K molecular and atomic gas, pink/red $\sim 10^4$–10^5 K warm ionized gas, and yellow/white $\gtrsim 10^6$ K hot gas. Gravitational collapse forms GMC and protostar cluster complexes throughout the gas. The outflows present include a component in dense clumps. Images of the other simulations at various times are in Appendix A.

Figure 2. The stars at the same time as Fig. 1. The image is a mock *ugr* (SDSS-band) composite, with the spectrum of all stars calculated from their known age and metallicity, and dust extinction/reddening accounted for from the line-of-sight dust mass. The brightness follows a logarithmic scale with a stretch of $\approx$2 dex. Young star clusters are visible throughout the system as bright white pixels. The nuclei contain most of the star formation, evident in their saturated brightness. Fine structure in the dust gives rise to complicated filaments, dust lanes and patchy obscuration of star-forming regions. A few super star clusters are apparent as the brightest young stellar concentrations. Images of the other simulations at various times are in Appendix A.

observed image, specifically a *u/g/r* composite. The stellar luminosity in each band is calculated from each star particle according to the STARBURST99 model, given its age, mass and metallicity (and smoothed over the appropriate kernel). We then attenuate the stars following the method of Hopkins et al. (2005): we calculate the total dust column (from the simulated gas) along the line of sight to each star particle for the chosen viewing angle (assuming a constant dust-to-metals ratio, i.e. dust-to-gas ratio equal to the MW value times $Z/Z_\odot$), and apply a MW-like extinction and reddening curve (as tabulated in Pei 1992).[4]

As seen in Paper II for isolated galaxies, gravitational collapse forms GMC complexes in the gas, which are individually dispersed rapidly by feedback once they turn a few per cent of their mass into stars, but are replaced by continuously forming new clumps. The ISM as a whole is a highly supersonically turbulent multiphase medium, with volume-filling hot gas (heated by SNe and O-star winds) making up a few per cent of the mass, a 'warm' phase of gas maintained by H II photoheating at $\sim 10^4$ K, which constitutes a large filling factor and mass fraction at large radii from the galaxy nuclei, and GMC complexes in dense molecular filaments (and volume-filling molecular gas near the galaxy centres), with most of the gas mass.

Violent outflows are clearly evident and are highlighted in Fig. 3, emerging both from individual GMC and from the merging systems as a whole. The composition of these outflows is discussed in detail in Paper III. Briefly, the volume-filling hot gas is primarily venting SNe and O star wind heated gas; there is some contribution from gravitational shocks, but it is much smaller (see Cox et al. 2006a and discussion below). Occasionally, the early stages of these outflows are evident as 'bubbles' breaking out of the warm phase gas. The warm/cold clumps embedded in the outflow predominantly come from material directly accelerated by radiation pressure (which is much more efficiently at launching cold gas out of the disc, as opposed to the entrainment of that cold material by hot, tenuous outflows).

In the stellar images, young star clusters are visible throughout the galaxies. Most of the stars form in resolved clusters; in a companion paper, we discuss the nature and properties of these clusters in detail. Most of them, however, are open clusters that correspond to GMC which have converted $\sim$5–10 per cent of their mass into stars (see Paper II), and so are unbound once the much larger (marginally bound) GMC gas mass is dispersed by feedback. The bright nuclei contain most of the star formation, as discussed below. The massive gas inflows give rise to large dust column densities along many sightlines; face-on, we see heavily extincted dust lanes with complex structure (filaments, feathering, etc.). The patchy obscuration is typical of local merging systems. A few super star clusters are visible as the brightest young stellar 'knots,' often outside the nuclei in tidally shocked arms.

---

[4] Accounting for dust scattering changes the detailed spectrum, but the colours and morphologies in the images are not significantly altered (Jonsson et al. 2006; Wuyts et al. 2009, 2010).
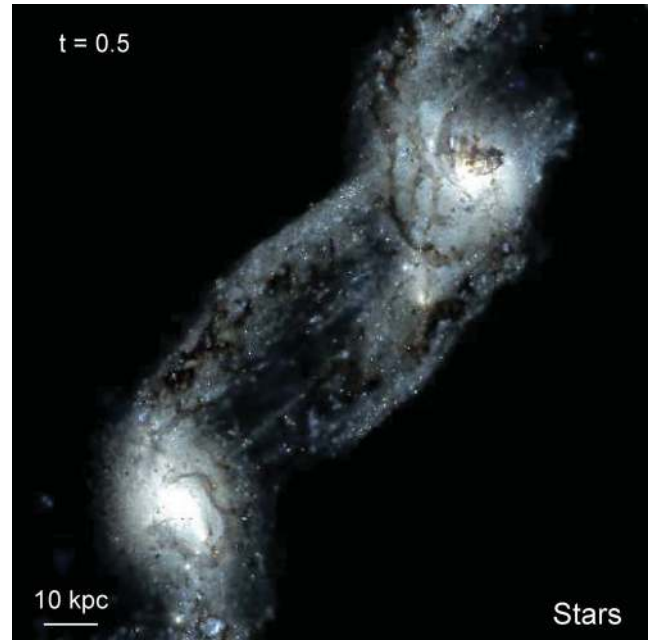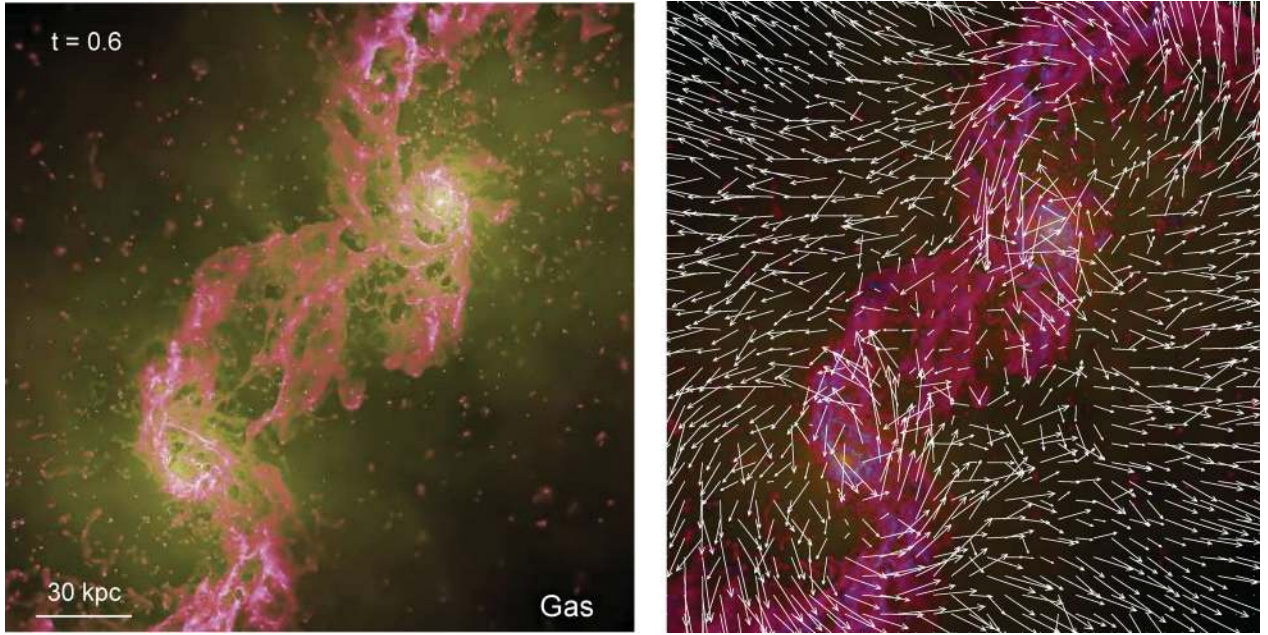
Figure 3. Left-hand panel: gas, as in Fig. 1, at a slightly later time, with a colour projection here chosen to emphasize the ionized and hot gas. Brightness now increases with surface density; colour encodes temperature in a similar manner (blue/pink/yellow representing the cold/warm/hot phases). Violent outflows are present, emerging both from the complexes and from the system as a whole, driven by the massive starburst. The volume-filling 'hot' component is now visible, with multiple 'bubbles' driven by separate local events. Right-hand panel: same, but with the (projected in-plane) velocity vectors plotted. The vectors interpolate the gas velocities evenly over the image; their length is linearly proportional to the magnitude of the local velocity with the longest plotted corresponding to $\approx 500\,\mathrm{km\,s^{-1}}$.
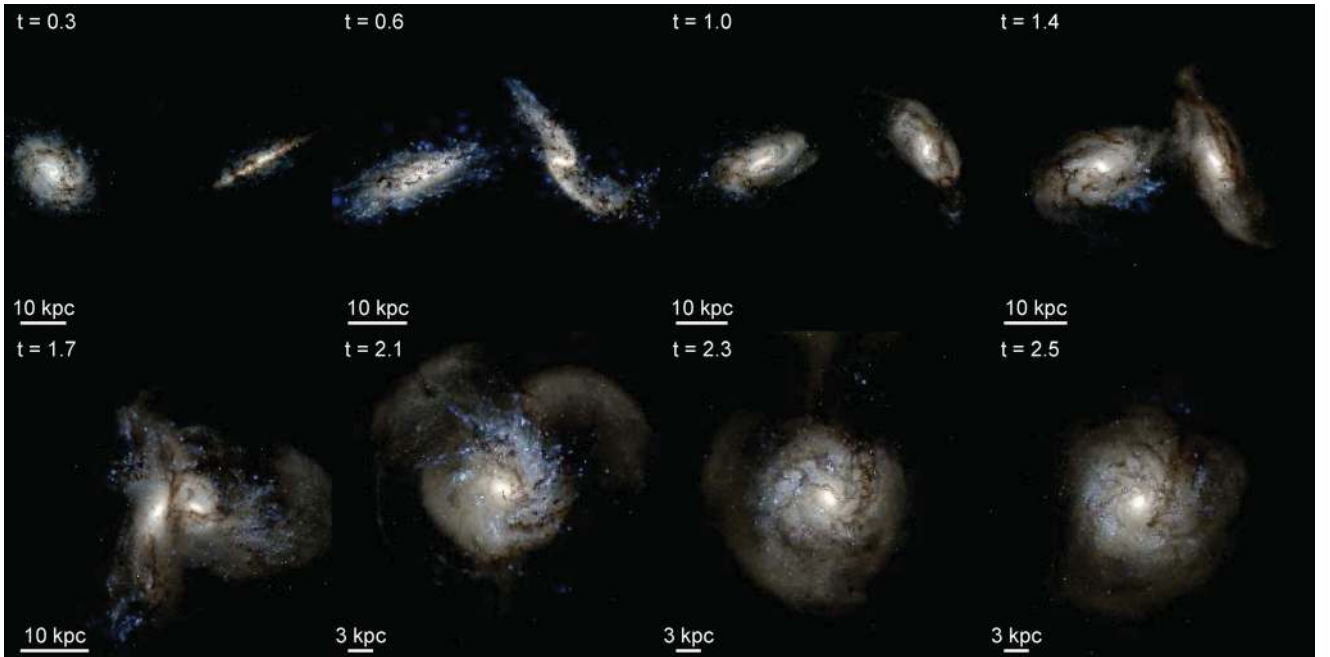
Figure 4. Morphology of the f (retrograde) merger of the Sbc galaxy (a dwarf starburst); each shows the optical as Fig. 2 at different times during the merger.

3.2 Merger remnant morphologies

As expected for the remnants of very major (equal-mass) mergers, the relic stars typically form a bulge-dominated galaxy once the merger has completed. In Fig. 6, we show this quantitatively by comparing the surface stellar mass density profiles of the remnant stars. We plot the median profile averaged over 1000 lines of sight

uniformly sampling the unit sphere, but the sightline-to-sightline differences are small. Despite being initially disc dominated, the HiZ and MW models form clear $r^{1/4}$-law bulges; the SMC and Sbc cases may still have significant discs (discussed below), evident in the curvature (lower Sérsic n_s) here.

The final mass profiles of models with explicit feedback or with an effective EOS are quite similar. This is, of course, expected
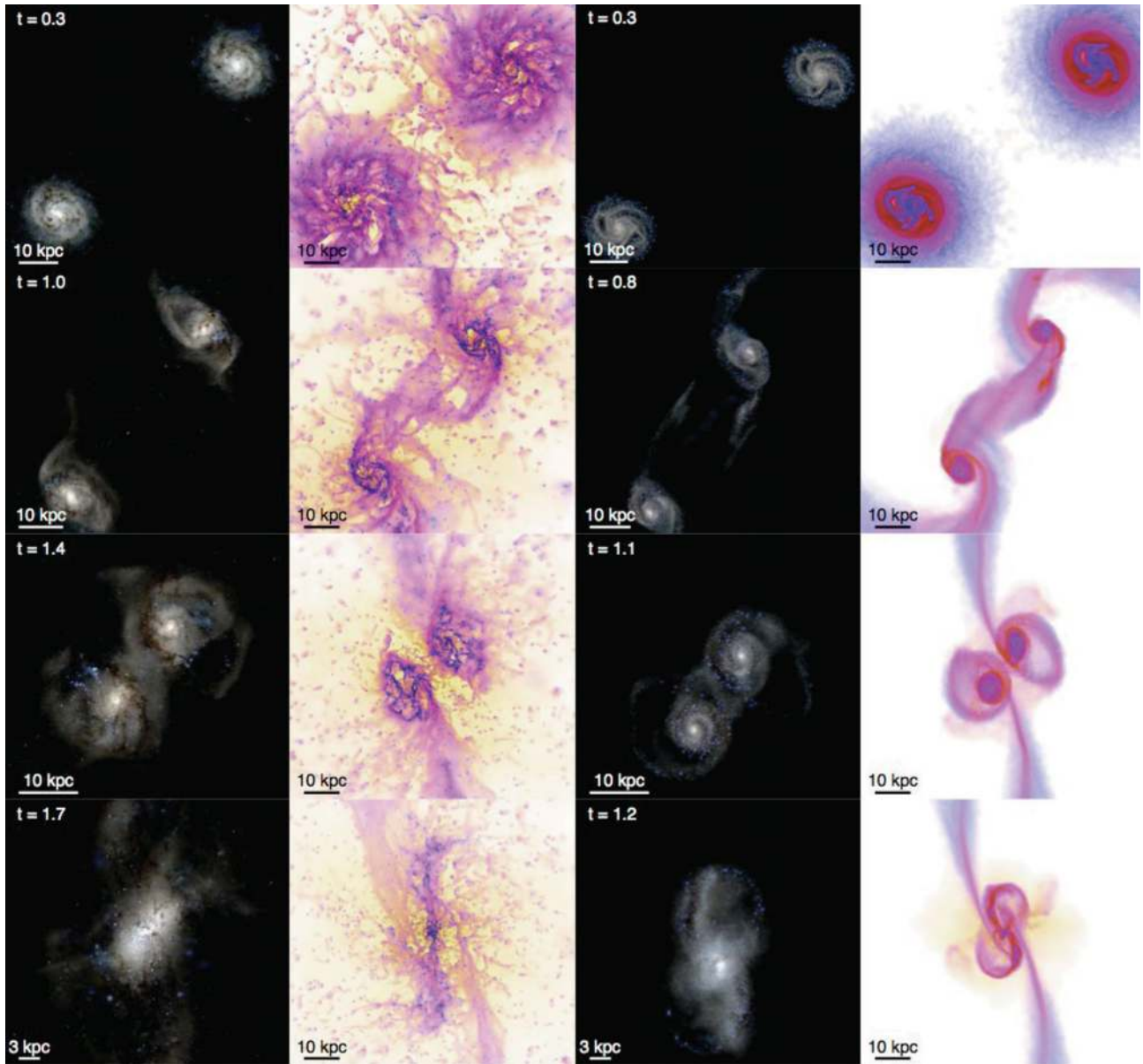
Figure 5. Comparison of the morphology in gas and stars in the *e* (prograde) merger of the Sbc (dwarf starburst) galaxy; each shows the optical and gas as Figs 1–4 at different times during the merger (top to bottom: before the first passage, after the first passage, before the final coalescence and after the final coalescence, respectively). Left-hand panels: simulations with explicit stellar feedback models (stars and gas). Right-hand panels: simulations with a simplified subgrid treatment of the ISM and stellar feedback; the lack of small-scale structure (molecular clouds, star clusters and dust lanes) and galactic winds is apparent. A complete set of images for all the simulations (with additional panels) is given in Appendix A.

where the profile is dominated by violent relaxation of pre-existing stars. However, in previous EOS models, it has generally been found that the central ~kpc is dominated by stars formed in situ in the nuclear starburst (from gas driven to the centre by strong torques; see Mihos & Hernquist 1994a; Hopkins et al. 2008c). We therefore examine the mass profile of two subcomponents: the stars formed in the starburst,[5] and the violently relaxed 'envelope' of stars formed before this starburst/coalescence (all stars formed previous to this cut). In all cases, the explicit feedback models are nearly identical to the 'effective' EOS models. In particular, the starburst component,

not just the dissipationless envelope, appears to have similar mass, shape and radius.

There are some systematic second-order differences. The full-feedback models tend to produce a somewhat more massive ~kpc-scale core (at the tens of per cent level), because dissipation is more efficient. There are subtle differences at large radii (~10 kpc) owing to extended star formation (discussed below), although the total stellar mass in young stars involved at these radii is very small.

3.3 Disc survival

A controversial subject in recent years has been the question of disc 'survival' or 're-formation' after mergers. Simulations with EOS models predicted that sufficiently gas rich mergers should

---

[5] For simplicity, we define this as all stars formed within ±150 Myr of the peak in the SFR near coalescence, but small changes in the definition have no effect on our conclusions.
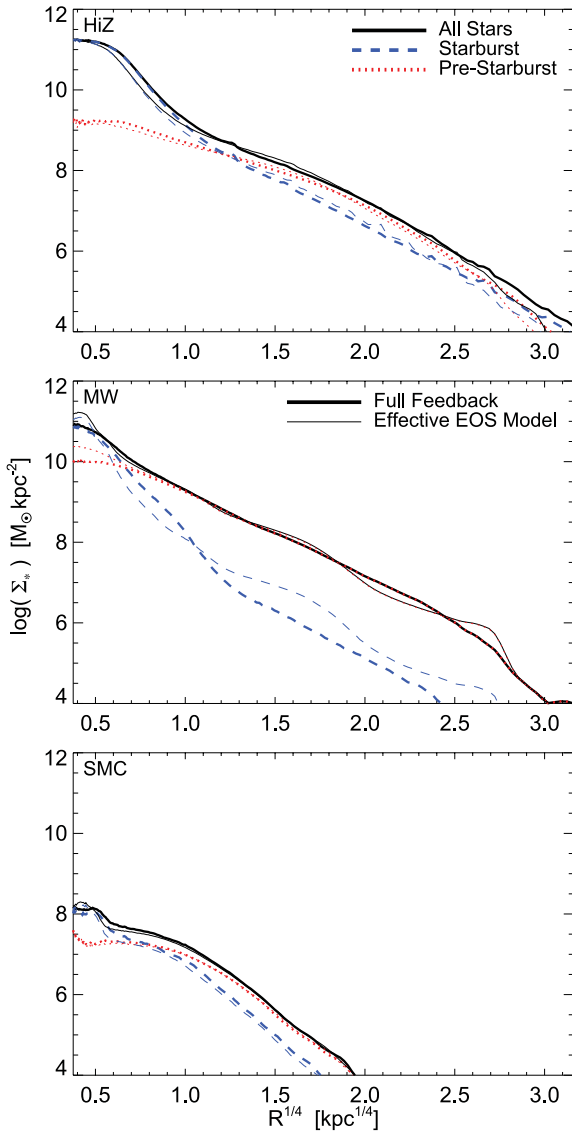
Figure 6. Merger remnant stellar mass profiles, with explicit (thick lines) and implicit/subresolution (thin lines) stellar feedback prescriptions. Top panel: high-redshift gas-rich starburst merger. Middle panel: MW-like galaxy merger. Bottom panel: SMC-mass dwarf merger. For each simulation, we plot the total stellar surface density (black solid), and the separate dissipationless/violently relaxed component (stars formed before the merger simulation; red dotted line) and dissipation/starburst component (stars formed in the merger-induced starburst; blue dashed line). The profiles are averaged over ≈100 viewing angles. In all cases, the profiles agree very well independent of the details of the feedback prescription. Despite the inner structure, dynamics and winds associated with the starburst being modified considerably, the 'total starburst mass' and characteristic radii where the post-starburst light dominates the profile appear robust. This is expected if these properties are set by large-scale gravitational torques.

leave large relic discs and even disc-dominated galaxies (Springel & Hernquist 2005; Robertson et al. 2006a; Hopkins et al. 2009b). Hopkins et al. (2009b) showed that in those models, this is governed by global gravitational torques being inefficient at removing angular momentum from gas at large radii in discs, and so is independent of the details of the EOS implementation or introduction of an ad hoc stellar wind model. However, other simulations, with either no hydrodynamics ('sticky particle' codes) or weak stellar feedback but

efficient cooling, predict much less efficient disc survival (Bournaud et al. 2011). We therefore examine this question for the first time in simulations with more detailed stellar feedback models.

Fig. 7 shows the morphology of one merger remnant (the SMC–SMC retrograde f merger) which clearly re-forms a prominent, rotationally supported disc. We quantify the disc mass and rotational support following Hopkins et al. (2009b), by plotting the distribution of baryonic mass as a function of its angular momentum j/j_c, where $j = |r \times v|$ is the specific angular momentum and $j_c = r [G M_{tot}(<r)/r]^{1/2}$ is the angular momentum of a circular orbit for each particle. The distribution is strongly bimodal, with a peak near zero net angular momentum (bulge stars), and a peak near $j/j_c = 1$, i.e. in a circular orbit. Fitting to this distribution (either cutting at the minimum between the two peaks or assuming the 'bulge' peak is symmetric about $j = 0$ and taking the 'disc' material as the residual material; see Hopkins et al. 2009b), we can identify the disc material as having an approximate rotational velocity of $\sim 40 \, \text{km s}^{-1}$ and mass of $\sim 5 \times 10^8 \, M_\odot$, in good agreement with the observed baryonic Tully–Fisher relation (Bell & de Jong 2001; McGaugh 2005). This is not to say our simulations uniquely predict this relation – it follows from the initial discs lying on the observed relation by construction – but it does say that the disc is a 'real' disc in as much as its progenitors were. Fig. 8 shows the optical image of the Sbc f merger relic, which also re-forms a prominent disc – based on the bulge-to-total mass ratio and presence of spiral arms, the face-on image is a typical Sa/b galaxy (edge-on S0/a).

The key question is the quantitative efficiency of survival. Since the behaviour of the dissipationless stars (i.e. how much they do or do not avoid violent relaxation) is identical in all models, we focus on the amount of gas which is able to survive the merger to re-form a disc. Hopkins et al. (2009b) parametrize this by examining the efficiency of gas consumption in the merger-induced starbursts. Gas which is not consumed (and not completely expelled by winds) will, inevitably, re-form a disc with whatever net angular momentum it carries (since it can cool). If all the gas were efficiently torqued (or locally forced to collapse in the merger), it would all contribute to the starburst, $f_{burst} = f_{gas}$ – there would be no 'residual' disc gas survival. Hopkins et al. (2009b) argue, however, that at high gas fractions these torques become inefficient so the burst fraction scales sublinearly with gas fraction as $\sim f_{gas}(1 - f_{gas})$; this is the origin of the enhanced survival in gas-rich mergers. We compare the explicit feedback models to the EOS models used to calibrate this relation, and find they are statistically nearly identical. The starburst efficiency is clearly well below $f_{burst} = f_{gas}$; i.e. disc survival is efficient. If anything, there is slightly *more* disc survival in these runs, compared to the EOS runs, owing to the contribution of winds expelling some of the mass that would have contributed to the starburst bulge.

4 STAR FORMATION HISTORIES

4.1 Starbursts

Fig. 9 shows the galaxy-integrated star formation histories of each simulation (averaged over ≈10 Myr intervals). The qualitative character of the models is similar, regardless of feedback details. In prograde (e) orbits, resonant interactions lead to starbursts on the first passage; however, since the models here have some pre-existing bulge, these are not always strong (Barnes & Hernquist 1991, 1996); they are less prominent in the retrograde (f) case because the systems are out of resonance. In all cases, there is a starburst on the final coalescence, as the gas is channelled to the galaxy centre.
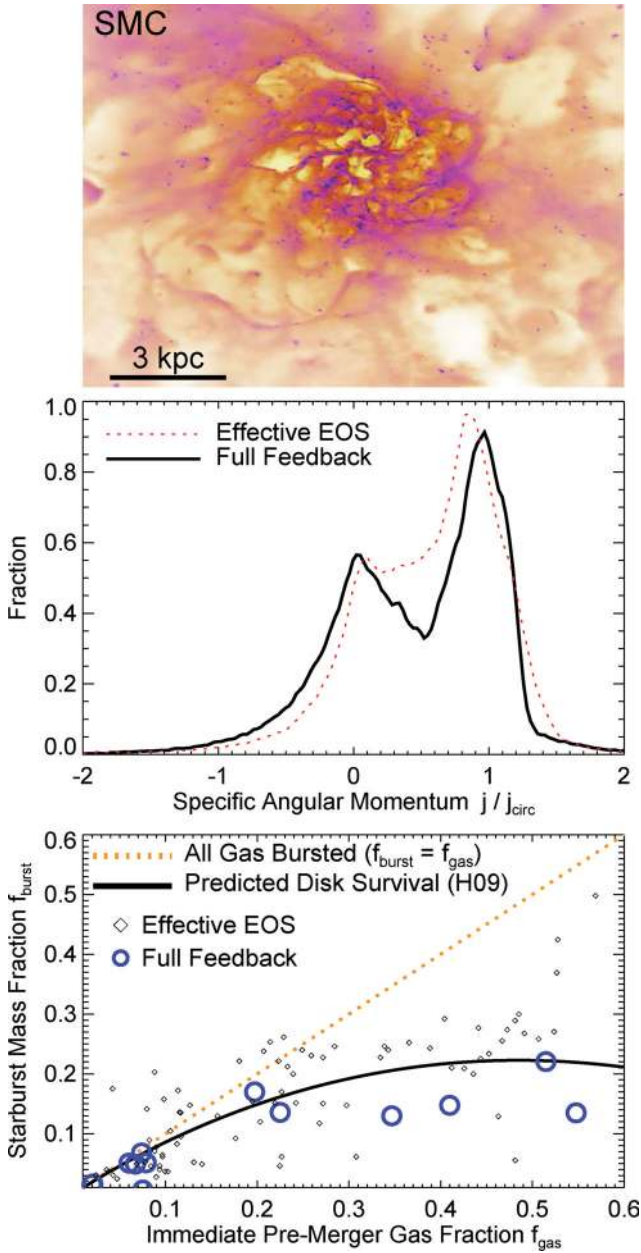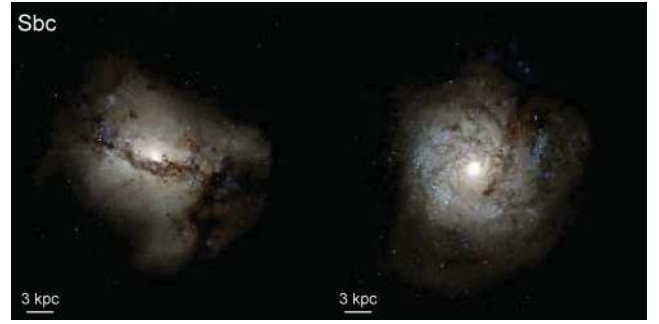
Figure 8. Optical image (as Fig. 2) of the stars in the relaxed merger remnant of the Sbc f merger (viewed edge-on and face-on). The violently relaxed stars form a very extended halo, but this is mostly at surface densities ~ 100 times smaller than the disc. The merger produces an S0/a (depending on the viewing angle), despite the fact that it just experienced an *equal-mass* (1:1) merger with no new gas accretion: most situations will give even larger discs.

The integrated mass in stars formed in total and in the major starburst(s) is similar, as suggested by Fig. 6. However, the exact maximum SFR and shape of the star formation history can differ significantly. It is already known that the duration, amplitude and variability within the starburst are quite sensitive to the initial conditions, and the treatment of the subgrid star formation recipe applied to the simulations (see Cox et al. 2006c), so this is not surprising.

In all explicit feedback models, there is increasing variability in the SFR, owing to star formation being concentrated in resolved GMC and clusters, and feedback being associated with individual star clusters (and SNe), hence more stochastic in time and space. Interestingly, this suppresses some of the differences between prograde and retrograde encounters in the weaker first-passage bursts, although quantifying this effect in detail requires a larger sample of orbits.

In the low-mass (SMC and Sbc) cases, the starbursts are much more pronounced with explicit feedback models; this is because the EOS models, even with effective sound speed $\sim 10\,\mathrm{km\,s^{-1}}$, are sufficient to highly pressurize the systems and suppress a strong burst. In this case, the allowance for molecular cooling makes the gas more compressible.

However, especially in the higher mass cases, expulsion of gas from the nuclei in feedback-driven winds (in the explicit feedback models) tends to 'spread' the starburst in time. In particular, it gives rise to a long tail of star formation as much of the material is not entirely unbound, but kicked into a fountain or stirred up within the disc and then re-condenses. The difference between this and the EOS case is especially clear in the prograde (*e*) models; there, with an EOS model, the gas is efficiently consumed in the starburst, leaving very little continuing star formation afterwards. However, in the explicit feedback models, the SFR declines from a similar peak much more slowly, remaining at more than an order of magnitude higher SFR for $\sim$Gyr.

This has important implications for 'quenching' of star formation in massive galaxies. If quenching were possible without the presence of some additional feedback source — say, from an active galactic nucleus (AGN) — then the simulations here are the most optimal case for this. They are isolated galaxies, so there is zero new accretion; moreover, an equal-mass merger represents the most efficient means to exhaust a large amount of gas quickly via star formation, much more so than an isolated disc (see e.g. Hopkins et al. 2008b,d). However, we find that with the presence of stellar winds, many of our models — including the already gas-poor MW-like
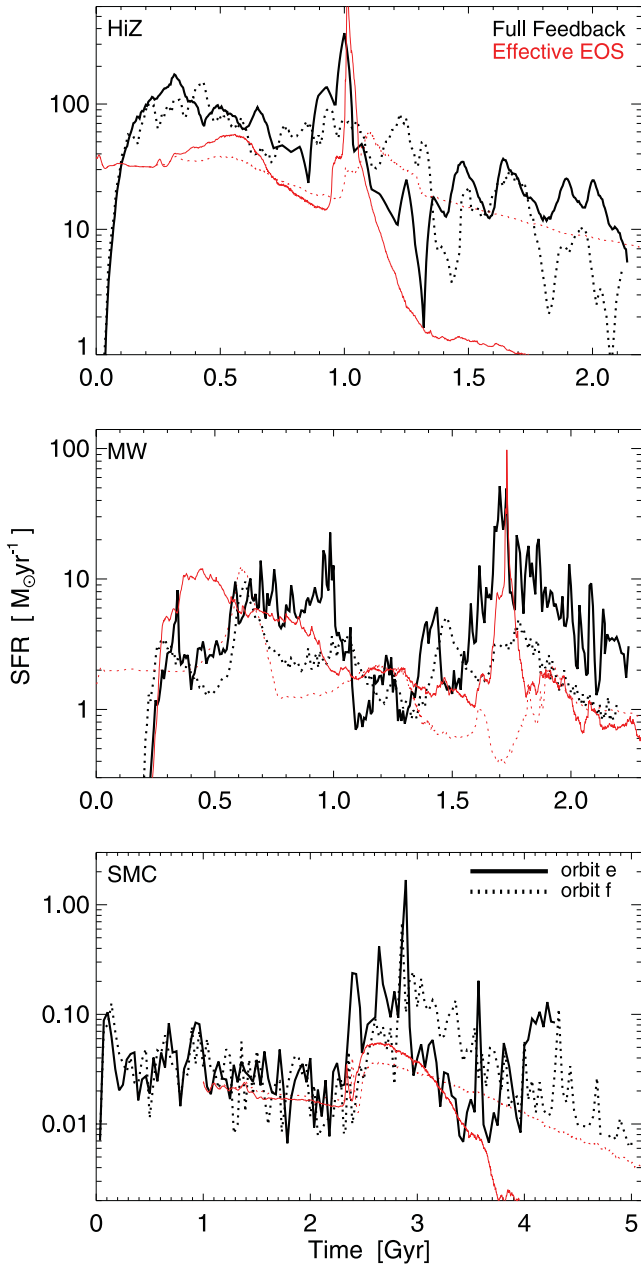

Figure 7. Disc survival in mergers. Top panel: gas image of the SMC f merger remnant (as Fig. 1), with our full-feedback model, after the final coalescence. The gas has clearly re-formed a large, rotating disc (face-on here), very similar to the isolated progenitor(s). Middle panel: distribution of specific angular momentum j of the baryons within 5 kpc of the centre of the same model, after the merger; values are compared to the value j_c of a pure circular orbit at the same radius. The distribution is clearly bimodal, with a peak containing ≈ 30 per cent of the mass near $j/j_c = 0$ (bulge), and ≈ 70 per cent in a peak near $j/j_c = 1$ (disc). The disc lies on the same Tully–Fisher relation as its progenitors. Bottom panel: mass fraction of the discs which is consumed in the final-coalescence starburst (f_{burst}), as a function of the gas mass fraction just before the burst begins (f_{gas}; here 200 Myr before the SFR peaks). The dotted line shows the result if all the gas were consumed, $f_{\mathrm{burst}} = f_{\mathrm{gas}}$. The solid line shows the approximate model for the efficiency of disc survival in gas-rich mergers from Hopkins et al. (2009b), roughly $f_{\mathrm{burst}} \approx f_{\mathrm{gas}} (1 - f_{\mathrm{gas}})$. The small diamonds compare the effective EOS simulations used to analyse disc survival therein. The large circles compare the simulations here. Values $f_{\mathrm{burst}} < f_{\mathrm{gas}}$ indicate disc survival and re-formation. Disc survival is comparably efficient in full-feedback and EOS models.

Figure 9. Star formation histories in some representative merger simulations, in EOS and explicit feedback models. In all cases, prograde (*e*) models produce more pronounced starbursts; the total mass consumed in the bursts is similar as well. The explicit feedback models predict more variable/bursty SFRs, because the ISM is less homogeneous. In low-mass systems, the bursts are much stronger with explicit feedback models, because the EOS models heavily pressurize the gas relative to the disc V_c (making it less compressible). At higher masses, the effect on the peak/duration of the starburst is more sensitive to other details. The 'tail' of post-starburst star formation is significantly enhanced in the explicit feedback models, especially in prograde mergers: in the EOS cases, the starburst gas is all exhausted efficiently, but with winds present; some of this is expelled into a fountain that continuously recycles gas for the next couple of Gyr. Starburst winds therefore make merger-induced quenching/gas exhaustion (at least without AGNs) *less*, not more, efficient.

system – maintain post-merger SFRs nearly as large as their steady-state pre-merger SFR. The systems simulated here would take several Gyr to cross the 'green valley' and turn red, much longer than the <Gyr quenching time-scale required by observations (see Martin et al. 2007; Snyder et al. 2011). Far from resolving this by gas expulsion, stellar feedback makes the 'quenching problem' *harder*.

As shown in Moster et al. (2011), addition of gas haloes around the merging galaxies (even without continuous accretion) only further enhances the post-merger SFR. Also, as shown in Fig. 9, the magnitude of the differences between models with and without the explicit stellar feedback models does depend significantly on the merger orbital parameters, so it may be possible that some orbits are 'more efficient' at exhausting gas than the limited pair we explore here. However, at least in these simulations, the smaller differences are seen in the retrograde orbits, i.e. the case where both models preserve significant gas throughout the merger, so it does not appear likely to resolve this issue.

Of course, the simulations here are not fully cosmological, so there may be other scenarios, such as a series of rapid mergers rather than a single major merger, which can exhaust gas and so terminate star formation more efficiently. However, if gas is to be swept out of galaxies efficiently after a merger, our models imply that some other form of feedback – perhaps from bright quasars – may be necessary. This is also suggested by observations of late-stage mergers, which find that in the AGN-dominated systems at quasar luminosities, outflow masses are enhanced and the outflow velocities reach ~1000 km s^{-1}, larger than those we find driven by stellar feedback (Tremonti, Moustakas & Diamond-Stanic 2007; Feruglio et al. 2010; Rupke & Veilleux 2011; Sturm et al. 2011).

4.2 The Kennicutt–Schmidt law

Fig. 10 plots the positions of the simulations with explicit feedback on the KS relation during the merger (the EOS models are placed on the relation by construction, and so are not interesting here). The agreement between these simulations and the observed relation for both isolated galaxies (the low-Σ_{gas} regime, corresponding to when the galaxies are well-separated discs) and observed merging ULIRG/starburst systems is excellent.

We remind the reader that there is no 'tunable' parameter in these models – the feedback strength is not adjusted to match the relation, and the instantaneous star formation efficiency we assign in self-gravitating gas is unity, not the ~1–2 per cent which is needed to match the Kennicutt relation. As we showed in Paper I and Paper II for isolated discs, the self-regulation of the SFR in these systems is a consequence of feedback; Paper I and Hopkins et al. (in preparation) show that their location on the Kennicutt relation has almost nothing to do with the actual star formation prescription, once feedback is included (but *is* sensitive to the strength of feedback, if we were to artificially adjust it). Also note that there is no evidence for bimodality in the relation, as suggested by Genzel et al. (2010) and Daddi et al. (2010); we discuss this in Section 6. In Paper I, we show that the observed 'cut-off' appears at sufficiently low Σ, but here it is less obvious since we always average over the half-SFR radius.

4.3 Where do stars form?

In Fig. 11, we plot the radii that enclose 50 per cent (R_{50}) and 90 per cent (R_{90}) of the star formation in the merging galaxies, as a
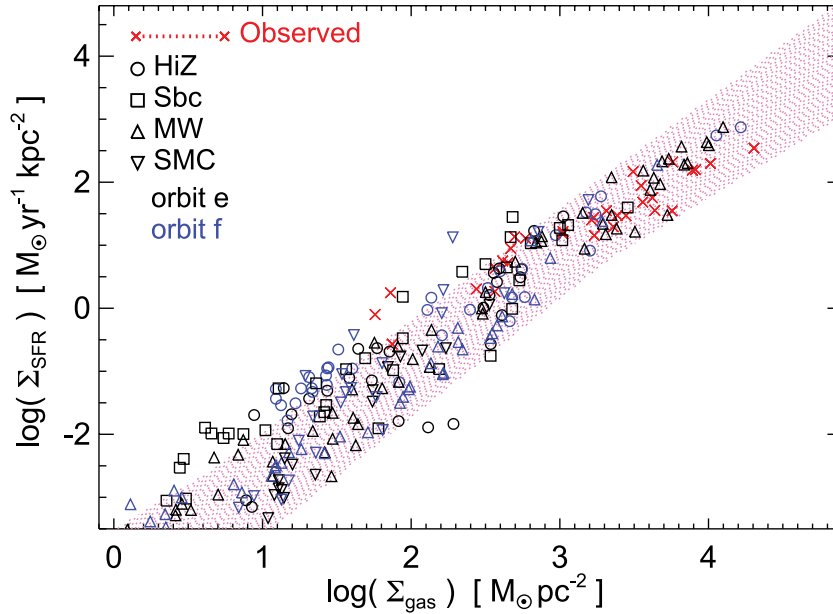
Figure 10. KS relation for the merger simulations with explicit feedback models. We compare the observed starburst galaxies in Kennicutt (1998) and updated with high-redshift galaxies by Genzel et al. (2010) (red × symbols); the shaded region shows the 90 per cent range at each Σ_{gas} from the compilations in those works, and Bigiel et al. (2008) and Daddi et al. (2010). Simulations are plotted at uniformly sampled times and with values measured at the half-SFR radius (averaged over 100 projections); before coalescence each merging galaxy is treated separately (populating the lower range). EOS models are constructed to lie on the relation by design, but the explicit-feedback merger models have a *local* star formation efficiency of unity in self-gravitating dense gas. Without feedback, the mergers lie a factor of ~20–100 above the observed relation (Paper I). With feedback – with no adjusted parameters – the KS law is well matched. As shown in Paper I and Paper II, this emerges generically from feedback self-regulating the SFR (independent of the small-scale star formation law); with the mechanisms included here, this extends even to extreme starbursts. There is no bimodality in the relation, though it may shift towards the upper envelope at high SFR.
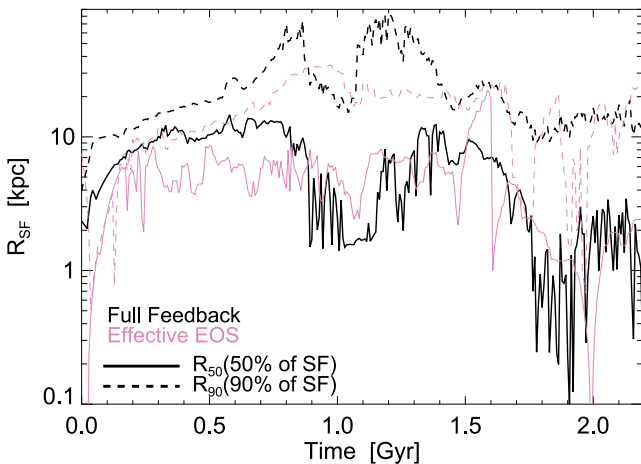

Figure 11. Radial distribution of star formation as a function of merger phase. For clarity, we focus on one example (MW *e*), but the others are qualitatively similar. We plot the radii enclosing 50 per cent (R_{50}) and 90 per cent (R_{90}) of the total SFR.[6]. In both EOS and full-feedback models, the half-SFR radius initially reflects the isolated discs, but drops to ~kpc due to inflows induced by global torques on the first passage, then to sub-kpc scales at the peak of the final-coalescence starburst. The 'compression' at the centre is slightly larger in the explicit feedback models because of cooling to low temperatures allowing higher densities. The outer extent of star formation (R_{90}) is generally similar, except leading into the first passage and between passages; here, more extended star formation in tidal shocks (in arms and the inter-galaxy bridge region) is captured in the full-feedback models, contributing ~20–40 per cent of the total SFR.

function of time.[6] At early stages, the radii are large – basically the values for the isolated discs as seen in Paper II. At the first passage, strong torques lead to shocks, dissipation, and rapid inflow; R_{50} drops rapidly as the gas piles up in an ~kpc-scale starburst. After this starburst, R_{50} increases again, until the final coalescence when new inflows are driven to small scales and most of the star formation comes from a sub-kpc nuclear starburst. This is the standard scenario of merger-driven starbursts in simplified EOS models as well (Hernquist 1989; Barnes & Hernquist 1991; Mihos & Hernquist 1994b, 1996).

The evolution of R_{90} is significantly different. At early times, it also reflects the isolated disc sizes. However, going into the first passage (especially just before the first-passage starburst), and between this starburst and the final coalescence, the radii actually become much *larger*, ~10–100 kpc. This is a consequence of star formation in tidal arms and the bridge region where the gas shocks between the two discs (especially prominent in prograde orbits). This is shown in Fig. 12, where we plot the morphology of the young stars for the same simulations. In these stages, ~20–50 per cent of the total SFR is contributed by this tidal/shock region. In contrast, it is well known that in models with a strong effective EOS, large density contrasts in shocks are poorly captured and so the SFR in these regions tends to be small, ~10 per cent of the total (see Barnes 2004; Karl et al. 2010). Even though strong feedback is present, the gas in these simulations is (at least instantaneously) more compressible,

---

[6] When the galaxies are well separated, we should consider the SFR within each separately; because our code is quasi-Lagrangian, we simply separate the particles belonging to each progenitor disc at all times, and take the appropriate radii separately (then plot the average of the two).
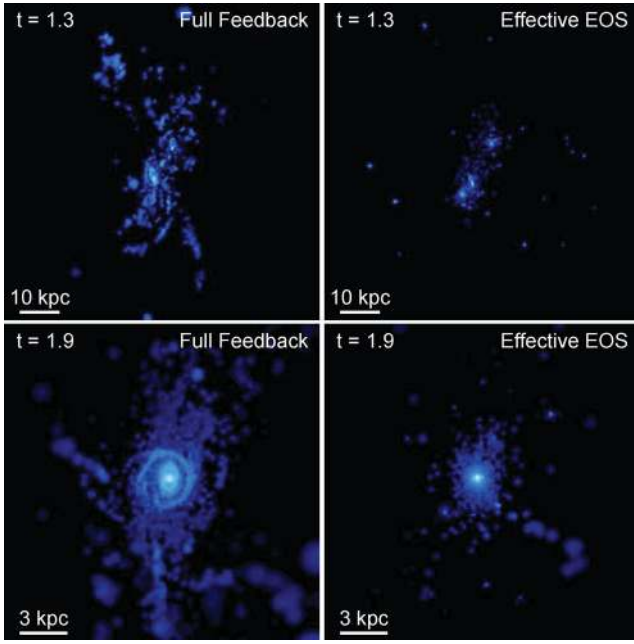
Figure 12. Morphology of the extended star formation plotted in Fig. 11, for the full-feedback (left-hand panels) and EOS (right-hand panels) models. We plot only the very young (<10 Myr old) stars (projected surface density increasing with brightness with an ≈2 dex stretch). We focus on the same example as Fig. 11 (MW *e*), at two times: just after the first passage (top panels) and near the final coalescence (bottom panels). The extended star formation is much more prominent in the full-feedback models, especially after the first passage in the tail/bridge regions. At the final coalescence, the kpc-scale starburst, hosting most of the star formation, has similar density and morphology in both runs, but is surrounded by more extended emission and a more prominent surviving star-forming disc in the full-feedback model.

so these shocks give rise to large density jumps that promote rapid star formation, significantly enhancing the contribution of the tidal region to the total SFR (seen in e.g. the no-feedback results with varied cooling prescriptions in Saitoh et al. 2009). This may be further enhanced at even higher resolution, with the ability to better resolve strong density gradients in shocks on sub-pc scales; however, at that scale, the effect of magnetic fields on shock compression is also important.

5 MODELS WITH WEAK OR NO FEEDBACK

In Paper I and Paper II, we discuss the properties of isolated simulations with no feedback. The models undergo catastrophic fragmentation with runaway gas collapse to arbitrarily high densities, turning most of the gas into stars in a single dynamical time. We have not focused on these models here, because they are clearly ruled out by, e.g. the observed Kennicutt (1998) relation. However, we briefly consider the differences between the predictions of the models here and a model with 'weak' feedback implemented. Specifically, we consider an effective EOS model with $q_{eos} = 0$, i.e. a cooling floor at 10^4 K or minimum turbulent velocity dispersion of 10 km s^{-1}. This is commonly adopted in historical models. This is not a no-feedback model; so it is not necessarily the case that the gas will experience runaway fragmentation. In the isolated MW or SMC models, this is comparable to the observed velocity dispersion and that predicted from our full-feedback model (see Paper II). However, in more extreme systems – the mergers here, and even the isolated HiZ models

– this is smaller than the predicted dispersions and the turbulent support needed to resist runaway gas fragmentation.

Fig. 13 plots the SFR versus time (as Fig. 9), the half-SFR radius versus time (as Fig. 11), and the KS relation (as Fig. 10) for this model and our standard full-feedback model. To highlight the differences, we focus on the most extreme case: the HiZ model and *e* orbit. This reaches the highest gas densities, SFRs and gas densities of our simulations, so is most sensitive to the strength of feedback. With the weak-feedback model, runaway collapse cannot be prevented. Early in the simulation (even before the galaxies are fully interacting, and especially on the first passage), the gas undergoes catastrophic fragmentation and local clumps collapse to the highest resolvable densities ($\sim 10^6$ cm^{-3}), turning into stars rapidly. Because of this, the SFR is much higher on early passages than the final coalescence. However, even in that coalescence, gas collapses rapidly as soon as it collects in filaments, before it can reach the nucleus. The effective radius of star formation in this stage is $\sim$5–10 kpc, rather than the $\lesssim$1 kpc traditional 'nuclear starburst' we see in the simulations with full feedback; stellar clumps form during the inflow and then sink collisionlessly into the bulge.[7] As a result, the SFR is more flat in the final coalescence (the burst enhancement is suppressed). This also means that the high nuclear gas densities ($\Sigma_{gas} \gg 10^3$ M$_\odot$ pc^{-2}) observed in ULIRGs are not actually reached. The predicted SFR densities on the Kennicutt (1998) relation are uniformly an order of magnitude larger than observed (recall, the observations include high-redshift systems analogous to the models here). Since the initial effective EOS model is tuned to lie on this relation, this produces an apparent sharp bimodality in the relation. Finally, since there is no super-wind, the SFR declines rapidly post-merger (having exhausted all the gas and with little material at large radii to 'rain back in'). At the end of the simulation, we measure the efficiency of disc survival as in Section 3.3; the surviving/re-formed disc mass in the weak-feedback simulation is only $\sim$1/3 of the mass of the re-formed disc in the full-feedback simulation.

6 DISCUSSION

We have studied major galaxy mergers with explicit models for stellar feedback that can follow the formation and destruction of individual GMC and star clusters. Our models include star formation only at extremely high densities inside GMC, and the mass, momentum and energy flux from SNe (Types I and II), stellar winds (both 'fast' O star winds and 'slow' AGB winds) and radiation pressure (from UV/optical and multiply scattered IR photons), as well as H II photoionization heating and molecular cooling. As a first study, we focus on simple, global properties, and compare them to those obtained from previous generations of simulations which did not follow these processes explicitly but instead adopted a simplified 'effective EOS' subgrid model of the ISM.

We find that most global consequences of mergers are similar, in models with explicit feedback and resolved ISM phase structure, and simplified EOS models. Some details, however, can be rather different.

---

[7] Note that even during the final starburst, the total extent of the star-forming region in the full-feedback models is quite large, $\gtrsim$10 pc; quantitative comparisons between similar simulations and observations of high-redshift extreme starbursts (submillimetre galaxies) show that their spatial distributions agree well (see e.g. Younger et al. 2008b; Ivison et al. 2009; Narayanan et al. 2009, 2010).
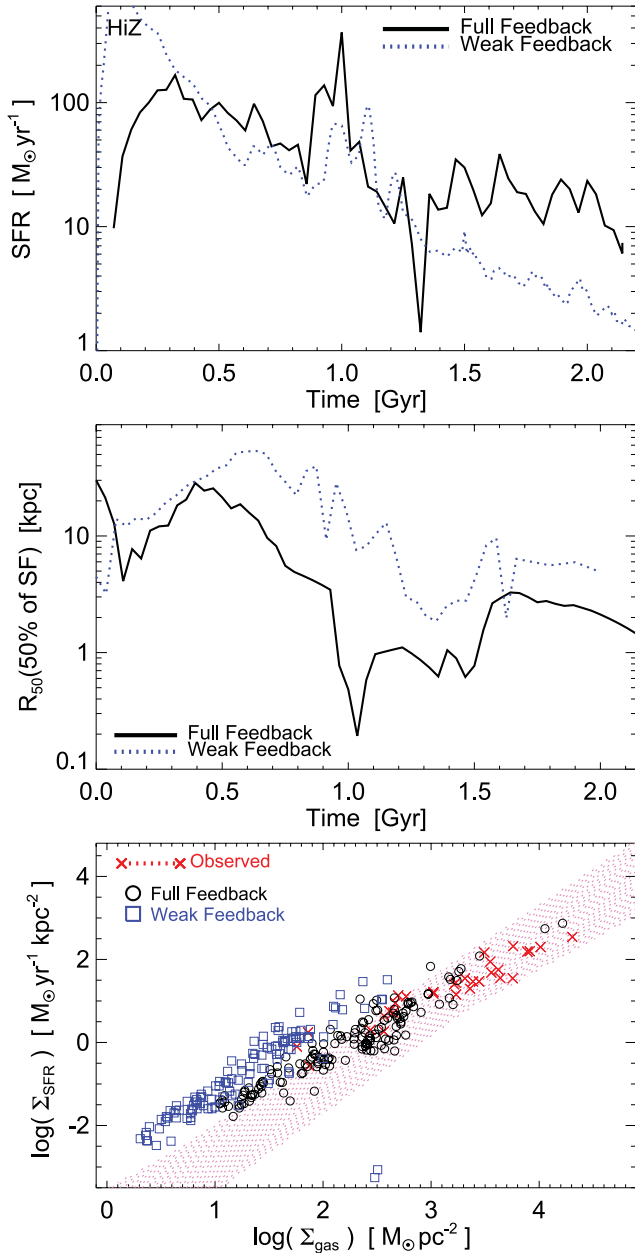
Figure 13. Comparison of a gas-rich merger with our full-feedback model to one with artificially weak stellar feedback. We compare our standard HiZ *e* model to a simulation with identical initial conditions but an effective EOS with $q_{eos} = 0$ (cooling floor at 10^4 K). Top panel: star formation history as Fig. 9. Without strong feedback, most of the gas is consumed by a massive burst within the discs when they begin to interact. The burst 'enhancement' in the final coalescence is much weaker. The post-merger SFR declines much more rapidly as the gas is exhausted, with no feedback-driven fountain to maintain gas infall. The surviving disc fraction is lower by a factor of ~3 in the weak-feedback model. Middle panel: half-SFR radius as Fig. 11. Even on coalescence, most of the SFR in the weak-feedback case comes from large radii $\gtrsim$5–10 kpc, as inflowing gas undergoes catastrophic fragmentation and turns into stars before it reaches the nucleus. With full feedback present, the dip in R_{50} at coalescence reflects inflows driving a starburst (as Fig. 11). Bottom panel: KS law as Fig. 10. With weak feedback, the highest observed surface densities (seen in merging nuclei) are never reached (gas fragments and turns to stars before reaching the central regions). The separated galaxies, constructed to lie on the KS law when isolated, also jump to much higher SFRs, predicting SFR densities an order of magnitude larger than observed and an apparently bimodal relation.

6.1 Galaxy morphologies

The relic structure and mass profile, and the presence of tidal tails in the merger, are predominantly determined by global gravitational torques, and so depend little on feedback details. This includes the integral properties (mass and effective radius) of the stellar relic of the kpc-scale starburst.

Mihos & Hernquist (1994a) argued that merger remnants are really two-component systems, and Hopkins et al. (2008c, 2009a,c) and Hopkins, Cox & Hernquist (2008a) later demonstrated this in comparison of observations (of ellipticals and recent merger remnants) and simulations with subgrid feedback models. The outer profile is dominated by violently relaxed stars formed before the final galaxy merger, which are dissipationlessly scattered into the 'envelope' at large radii. The inner portion is dominated by 'starburst' stars which form via gas that is gravitationally torqued and dissipates, falls to the centre, and turns into stars in a central starburst; this dominates the central ~kpc and extends inwards to form the central 'cusps' in gas-rich merger remnants (see Kormendy & Sanders 1992; Hibbard & Yun 1999; Rothberg & Joseph 2004; Hopkins & Quataert 2011b); it is often responsible for nuclear kinematically decoupled components (Hernquist & Barnes 1991; Hoffman et al. 2010).

We find that this decomposition, and the behaviour of the mass profile of each subcomponent separately (as well as the total), is robust to the inclusion of explicit or effective EOS models. This is reassuring, since Hopkins et al. (2008c, 2009a) showed that the simulated mass distributions agree very well with observed mergers and spheroids, and Cox et al. (2006c) showed these results are robust to substantial changes in subgrid parametrizations of feedback and star formation. The dissipationless profile should obviously be insensitive to the gas physics. The dissipative profiles are similar because, as shown in Hopkins et al. (2008c), their characteristic radii are set not by feedback 'pressurizing' the material, but by the radius at which the inflowing gas becomes self-gravitating, at which point it is no longer strongly torqued by the external stars and dark matter and can turn into stars relatively rapidly. The slope of the central mass profile is set by equilibrium between gravitationally driven inflow and star formation (Hopkins & Quataert 2011b).

We may, however, expect differences in very low mass, gas-rich mergers. In the EOS models, these are 'pressurized' to the point where the effective sound speed is comparable to the circular velocity, and so tend to result in merger remnants that are larger compared to true ellipticals at $\lesssim 10^9 M_\odot$ (Hopkins et al. 2009a). Allowing the gas to be more compressible (instantaneously), while retaining feedback, may resolve this discrepancy.

6.2 Disc survival

Disc survival – the efficiency with which gas avoids consumption in the merger and can rapidly re-form a disc after – appears to be just as, if not slightly more, efficient in models with explicit feedback (appropriately accounting for their properties at the time of merger). They follow the same scalings for the likelihood of disc survival (and gas angular momentum loss) as derived from simplified models in Hopkins et al. (2009b).

This is expected: Hopkins et al. (2009b) found disc survival did not depend on the subgrid parameters of the EOS model (unless feedback is very weak), and discuss the reasons for this. Gas is dissipative, so gas that survives the merger without turning into stars or losing most of its angular momentum will eventually re-form a rotating disc. The dominant torques driving angular momentum loss

in mergers arise from resonant interactions exciting collisionless perturbations in the stars, which in turn force the gas into strong shocks (Barnes & Hernquist 1991, 1992; Barnes 2002; Hopkins & Quataert 2010, 2011a). Angular momentum 'cancellation,' viscosity, other hydrodynamic torques, and the direct torque from the presence of the secondary galaxy are typically much smaller effects. As a result, one can analytically derive a critical radius and resonant conditions that depend only on merger orbit, mass ratio and galaxy structural properties (not the gas microphysics), outside which gas will not be strongly torqued and will thus survive to re-form discs. With few stars, gas-rich discs have weak collisionless torques, so give larger surviving discs.

The same has also been seen in cosmological simulations with subgrid feedback models (Governato et al. 2009, 2010; Guedes et al. 2011). Discs survive multiple major mergers by virtue of conserving gas which immediately re-forms discs; this is enhanced by the presence of feedback-driven outflows which further suppress the mass turned into stars in the centre. This is important for the existence of 'realistic' discs today (Robertson & Bullock 2008; Hopkins et al. 2009e; Stewart et al. 2009), and there appear to be a growing number of observed discs that have undergone recent mergers (Bundy et al. 2009, 2010; Hammer et al. 2009a,b; Puech et al. 2009; Yang et al. 2009).

6.3 Starbursts and star formation

The final starbursts are dominated by in situ star formation from gas which is torqued, falls into the nucleus and turns into stars at high densities. This is the 'standard' scenario of merger-driven nuclear starbursts and star formation predicted in early simulations (Barnes & Hernquist 1991; Mihos & Hernquist 1994b, 1996), and observed at the centres of nearby ULIRGs (strong, rapid inflows evident in their profiles of molecular gas, star formation and metallicity; see e.g. Kormendy & Sanders 1992; Sanders & Mirabel 1996; Titus, Spillar & Johnson 1997; Hibbard & Yun 1999; Reichardt, Jimenez & Heavens 2001; Tacconi et al. 2002; Rothberg & Joseph 2004; Michard 2006; Sánchez-Blázquez et al. 2007; Foster et al. 2009; Kewley et al. 2010; Rupke, Kewley & Barnes 2010; Soto & Martin 2010). Cox et al. (2006c) showed that this is robust to large variations in the implementation of feedback in subgrid models. As emphasized in many previous studies, we are not saying that most of the stars form in the starburst: this is typically ∼10 per cent of the total stellar mass (Jogee et al. 2009; Robaina et al. 2009; Hopkins et al. 2010; Hopkins & Hernquist 2010), with the rest formed in the 'isolated disc' mode (including times during the merger outside the 'burst').

Although gas clumps (into GMC) as it flows in, feedback efficiently disperses these GMC after they turn just a few per cent of their mass into stars. However, the material is not expelled completely (which would shut down the burst entirely); most of the recycled gas is unbound *locally* from the GMC, but not globally from the galaxy. The typical velocities are the escape velocities from the GMC or local star cluster (∼10 km s^{-1}) and so the gas is 'stirred.' This allows it to reach the nuclei in a coherent flow, so that gravitational torques will still tend to dominate.

The more explicit feedback models, however, show significantly higher star formation in tails and bridges (especially in shocks). This may resolve a long-standing discrepancy between merger models and observed star formation distributions in local mergers (Barnes 2004); a more quantitative comparison with models intended to mimic these specific systems will be the subject of future work.

In the explicit feedback models, the star formation is more strongly time-variable (less 'smoothed' by the effective EOS). This owes to the more inhomogeneous nature of the ISM – in extreme cases, a large fraction of the SFR can come from a few super star clusters. The burst 'enhancement' (peak SFR) can be higher or lower, depending on the orbit and structural properties; as with subgrid models, first-passage bursts are much more sensitive to these details than the final coalescence. In low-mass systems, it tends to be higher, because (as noted above) the EOS models may overpressurize small discs by enforcing a minimum sound speed of ∼10 km s^{-1}; with molecular cooling, the gas can more efficiently collapse to high densities in the nucleus.

In all the explicit feedback cases, the 'tails' of the starburst tend to be more broad; this owes to the effect of stellar winds ejecting some material at modest velocities, so it falls back into the disc in a fountain and makes the starburst more extended (discussed below).

6.4 The Kennicutt–Schmidt relation

The explicit feedback models predict SFRs that agree extremely well with observed merging galaxies on the KS relation. This is a major success of the models: unlike the EOS models, where the kpc-scale star formation law is imposed to match the Kennicutt law, the predicted Kennicutt relation in the explicit feedback cases is a true prediction (in normalization, scatter and power-law slope). Recall, star formation in these models occurs only in very dense, locally self-gravitating gas (scales ≲pc), with an instantaneous local efficiency of unity – not the global ∼1 per cent value of the Kennicutt relation, and without feedback (see Paper I and Paper II), the models predict a SFR far larger than observed, $\dot{M}_* \sim M_{\mathrm{gas}}/t_{\mathrm{dyn}}$. With feedback included – with parameters not in any way adjusted to reproduce the observations but taken directly from stellar evolution models – the observed relation naturally emerges.

This is a consequence of feedback-regulated star formation: turbulent support in the gas dissipates locally on a crossing time, leading to collapse, which proceeds until a sufficient number of young stars form (regardless of *how* they form, in detail) to provide enough momentum flux in feedback to balance the dissipation. As such, we showed in Paper I that the SFR and Kennicutt relation are direct consequences of feedback, and are *independent* of the microphysical star formation law once explicit feedback is included. We find the same here; we have re-run some of our simulations replacing our local self-gravity criterion for star formation with a simple density threshold with a very different efficiency (or changing the small-scale density dependence), as discussed in Section 2, and the predicted Kennicutt law is nearly identical.

The same feedback mechanisms regulating star formation in isolated galaxies extend to the regime of extreme merger-induced starbursts. This is no mean feat: the typical surface densities and SFRs are orders of magnitude larger than the isolated disc counterparts of these galaxies. The gas surface densities in the bursts here extend to ∼100–1000 times larger than the mean surface density of local GMC! We are therefore well into the regime where the medium is entirely molecular and of high density (although it may still exhibit phase structure). In Paper II, we showed that SNe and other 'thermal' feedback mechanisms become unimportant in gas above densities ∼1–10 cm^{-3} (typical of the diffuse gas in GMC), because the cooling times are extremely short compared to the dynamical times. We therefore expect that radiation pressure is the most important feedback mechanism in these starburst regions, as we found there for the most dense regions within 'normal' GMC. It is a remarkable success of the models, though, that they interpolate

naturally into even this extreme regime, without requiring any adjustment. In contrast, most analytic models for the KS relation have been forced to assume some ad hoc break or transition in the scaling at high densities.

We see no strong bimodality in the predicted relation. However, this is not necessarily inconsistent with recent observational claims along these lines (Daddi et al. 2010; Genzel et al. 2010); our merger and isolated galaxy simulations overlap closely with the observations from those papers. What we see is a continuum between these systems, which is completely consistent with the observations (see e.g. Narayanan et al. 2011). The apparent bimodality stems from a strict choice of two separate CO conversion factors; in future work, we will incorporate detailed models for molecular emission to make a quantitative comparison with these observations. Narayanan et al. (2012) find that when applying a functional form for the $CO-H_2$ conversion factor which depends on the physical conditions in the ISM to the observed galaxies in Fig. 10, a slope of ~ 1.8 emerges. Our results are quite consistent with those, and we find a slope of ~ 1.7; this suggests that stars do form somewhat more 'efficiently' (in terms of consumption time) in systems like mergers which occupy the high surface density region of the KS plot, though mergers do not lie on a different track of the relation from discs. The increased efficiency likely owes to a larger fraction of gas in the dense phase, a result which has been noted in observations of local ULIRGs (e.g. Juneau et al. 2009).

6.5 Comparison to models with weak feedback

Recently, there have been some different conclusions reached in the literature from the study of high-resolution simulations with very different implementations of stellar feedback. Teyssier et al. (2010) argued that merger-induced starbursts might not occur 'in situ' from inflows, but instead from catastrophic fragmentation of tidal arms, bars, and other instabilities. The fragments would turn a large fraction of their mass into stars very rapidly, and then sink as supermassive stellar clusters to the galaxy centre via dynamical friction, building the bulge. They also suggest a sharp bimodality in the KS relation, with the mergers and isolated discs being well separated, as a consequence of this induced fragmentation in the mergers (though they do discuss how this might be smoothed out). Bournaud et al. (2011) argued that disc survival is very inefficient in their simulations, for similar reasons – the gas undergoes dramatic fragmentation and 'clumps' scatter off one another, providing new torques.

We believe that these differences stem from the fact that these simulations include relatively weak stellar feedback, which is unable to disperse dense gas clouds (GMC and especially clouds in the dense tidal or starburst regions of mergers) after they form. In fact, we reproduce these results if we re-run our mergers with an effective EOS model with much weaker 'feedback strength,' $q_{eos} = 0$. Like the $q_{eos} = 0$ models, the Teyssier et al. (2010) models adopt an effective EOS, but one in which the 'median' ISM temperature is much colder than the subgrid sound speeds used in the EOS models here, which makes catastrophic fragmentation possible. Without strong feedback, the clumps cannot then disperse and recycle their mass. Specifically, the models either do not include explicit feedback mechanisms or include only SNe; however, we found in Paper I and Paper II that SNe have little effect on the dispersal of dense gas, because the cooling time in that gas is much shorter than the dynamical time. As a result, the SNe can stir up the 'diffuse' medium but cannot recycle dense gas. In our simulations, the most dense clouds are destroyed by a combination of radiation pressure in both the UV and the IR, photoionization, and momentum from O star winds.

In models that allow cooling but do not include these explicit feedback mechanisms, therefore, gas cools and collapses into dense GMC-like objects, which steadily contract and form stars, but are not efficiently 're-mixed' into the ISM on a short time-scale. Collapse (hence star formation) in the dense regions runs away, giving rise to the dramatically enhanced 'fragmentation mode' of star formation and apparent bimodality in the Kennicutt relation. In Paper II we show that even if slow star formation is forced in the dense regions, the lack of mixing allows the dense regions to move ballistically, with relatively small interaction cross-sections and long lifetimes. In this limit, gas is effectively no longer collisional. All the dissipation occurs within individual clumps, while the relative motions between clumps cannot be dissipated, just like relative motions of stars; the gas behaves like a collection of 'supermassive' stars or dark matter particles, and loses orbital angular momentum only via processes much slower than shocks, such as scattering and dynamical friction.

In contrast, observations suggest that GMC are short lived, with lifetimes of a few free-fall times (few Myr), and turn just a few per cent of their mass into stars before dispersing (Zuckerman & Evans 1974; Williams & McKee 1997; Evans 1999; Evans et al. 2009). Although the relevant physics in galaxy-scale simulations remain quite uncertain (and it is unclear how robustly this can be generalized to all the cases studied in this paper), short lifetimes do appear to be typical even for the most massive (10^8–$10^9\,M_\odot$) GMC complexes observed in local mergers (Rand & Kulkarni 1990; Planesas, Scoville & Myers 1991; Wilson et al. 2003, 2006). So even if most of the gas at a given instant is in dense subunits (GMC), the gas can be recycled through the diffuse ISM on a short time-scale, and therefore experience normal hydrodynamic forces. So long as the GMC lifetime is short compared to the total duration of the strong torques in the merger ($\sim 500\,Myr$), this will be true.

Likewise, since inflows in the final coalescence of a major merger require only a couple of dynamical times to reach the centre, for fragmentation to 'beat' inflow as a starburst driver the fragmenting clumps in the inflow would have to have a very high instantaneous star formation efficiency, $\dot{M}_* \sim M_{gas}/t_{dyn}$. This happens in models with weaker feedback; however, the observed Kennicutt relation in ULIRGs and other mergers (even high-redshift systems) implies an efficiency substantially smaller (by as much as a factor of ~ 50), and direct observations of ULIRGs do suggest that the final-coalescence SFR is indeed dominated by a nuclear starburst (see references above).

A key conclusion is that, in any model which resolves the formation of dense clouds, predictions critically depend on the physics that may (or may not) *destroy* those clouds.

6.6 Caveats and future directions

The results here are drawn from a preliminary study of how more detailed and explicit stellar feedback and ISM structure influence the results of merger simulations. We have found that the most basic global integral properties of star formation and galaxy morphology tend to be similar to those inferred in previous studies with a simplified treatment of the gas physics. However, we also find that more detailed structural and kinematic properties are sensitive to the gas physics. We do not expect this to be the case outside the central $\sim$kpc, where the relic galaxy is dominated by stars formed before the merger and violently relaxed. However, kinematic substructures in the central region may be sensitive to how the gas

collapses and turns into stars. It will also be particularly interesting to examine the effects of more detailed star formation and enrichment models that can separately follow stellar winds and SNe of Types I and II on the age, metallicity and abundance (α/Fe) gradients in the galaxies; these can place strong constraints on the merger history and role of dissipation in galaxy formation (see e.g. Torrey et al. 2012a, and references therein).

In a companion paper, we examine the star clusters formed in these simulations. The mass/luminosity distribution, spatial locations, formation time distribution and physical properties of these clusters represent a powerful constraint on small-scale models of the ISM and star formation.

We have also restricted our focus to major mergers. Studies of mergers with varying mass ratios suggest that the qualitative behaviours discussed here should not depend on mass ratio for ratios to about 3:1 or 4:1, and even at lower mass ratios they can be considered similar but with an 'efficiency' of inducing starbursts and violent relaxation that scales approximately linearly with mass ratio (Hernquist & Mihos 1995; Naab & Burkert 2003; Cox et al. 2008; Younger et al. 2008a). However, at small mass ratios the dominant role of mergers may be more subtle: inducing resonant disc perturbations (D'Onghia et al. 2009, 2010) and disc heating (Walker, Mihos & Hernquist 1996; Hopkins et al. 2008e; Stewart et al. 2008; Purcell, Kazantzidis & Bullock 2009; Moster et al. 2010), for which the gas response may depend significantly on its phase structure.

We note that recent studies comparing cosmological simulations done with GADGET and the new moving mesh code AREPO (Springel 2010) have called into question the reliability of smoothed particle hydrodynamics (SPH) for some problems related to galaxy formation in a cosmological context (Torrey et al. 2012b; Bauer & Springel 2012; Kereš et al. 2012; Sijacki et al. 2012; Vogelsberger et al. 2012). However, we have also performed idealized simulations of mergers between individual galaxies and found excellent agreement between GADGET and AREPO for gas inflow rates, star formation histories and the mass in the ensuing starbursts, for example, for reasons that will be discussed in Hayward et al. (in preparation). The discrepancies above are also minimized when the flows of interest are supersonic (as opposed to subsonic), which is very much the case here (Kitsionas et al. 2009; Price & Federrath 2010; Bauer & Springel 2012). We have also compared a subset of our merger simulations run with an alternative formulation of SPH from Hopkins (2013), which produces results much more similar to grid codes; in these tests, we confirm all of the qualitative conclusions here.

Our new models allow us to follow the structure of the gas in the central regions of starburst systems at high resolution. This makes them an ideal laboratory for studying feedback physics under extreme conditions in, say, the centre of Arp 220 and other very dense galaxies. In another companion paper, we examine the properties of the large starburst winds driven by stellar feedback in the mergers, which can reach $\sim$10–500 $M_\odot$ yr^{-1} outflow rates and so have potentially major implications for metal enrichment and self-regulation of galaxy growth. We have also here, for clarity, neglected AGN feedback in these models, but we expect it may have a significant effect on the systems and their outflows after the final coalescence. For example, it may strongly suppress the otherwise quite high post-merger SFRs we see in these simulations, which – without something to rapidly 'quench' them – may make it difficult or impossible to explain the observed abundance of high-redshift, low-SFR galaxies. With high-resolution models that include the phase structure of the ISM, it becomes meaningful to include much more explicit physical models for AGN feedback.

Finally, we stress that these models are still approximations, and the treatment of ISM and star formation physics is necessarily still 'subgrid' at some level (just at the GMC level, instead of the kpc level). We can follow galaxy-wide phenomena such as mergers, and large-scale processes such as the formation of GMC and massive star clusters. However, we still require assumptions regarding the behaviour of gas at densities above $\sim$10^4–10^6 cm^{-3}, and make simple approximations to the chemistry of the gas (especially at low temperatures); our feedback models also average over the IMF, owing to the fact that a single stellar particle still represents many individual stars, rather than discriminating individual low- and high-mass stars. The treatment of radiative feedback, in particular, is not a full radiative transfer calculation (which, for the IR, is extremely demanding and may be sensitive to very small scale unresolved ISM structure). It remains, unfortunately, prohibitively expensive to treat these physics much more explicitly in galaxy-wide simulations. As such, the behaviour of any individual molecular cloud or star cluster is at best marginally resolved in our simulations and should only be taken as a first approximation to the behaviour that might be obtained if the evolution of that system could be followed in detail. However, it is common to consider both these physics and much smaller spatial and mass resolution of substellar masses and <0.1 pc in simulations of the ISM and star formation within small 'patches' of the ISM. There is considerable and rapidly growing simulation work in these areas, much of it 'building up' to larger scales such as GMC, overlapping with our smallest resolved scales. This suggests that considerable progress might be made by combining these approaches and using smaller scale (but more accurate and explicit) star formation and ISM simulations to calibrate and test the approximations in galaxy-scale simulations such as those here, which can themselves, in turn, be used to calibrate the kpc-scale subgrid approaches still required for fully cosmological simulations.

REFERENCES

Barnes J. E., 1988, ApJ, 331, 699
Barnes J. E., 2002, MNRAS, 333, 481
Barnes J. E., 2004, MNRAS, 350, 798
Barnes J. E., Hernquist L. E., 1991, ApJ, 370, L65
Barnes J. E., Hernquist L., 1992, ARA&A, 30, 705
Barnes J. E., Hernquist L., 1996, ApJ, 471, 115
Bauer A., Springel V., 2012, MNRAS, 423, 3102
Baugh C. M., Lacey C. G., Frenk C. S., Granato G. L., Silva L., Bressan A., Benson A. J., Cole S., 2005, MNRAS, 356, 1191
Bell E. F., de Jong R. S., 2001, ApJ, 550, 212
Benson A. J., 2005, MNRAS, 358, 551
Bigiel F., Leroy A., Walter F., Brinks E., de Blok W. J. G., Madore B., Thornley M. D., 2008, AJ, 136, 2846
Bournaud F., Elmegreen B. G., Teyssier R., Block D. L., Puerari I., 2010, MNRAS, 409, 1088
Bournaud F. et al., 2011, ApJ, 730, 4
Bundy K., Fukugita M., Ellis R. S., Targett T. A., Belli S., Kodama T., 2009, ApJ, 697, 1369

Bundy K. et al., 2010, ApJ, 719, 1969

Burkert A., Naab T., Johansson P. H., Jesseit R., 2008, ApJ, 685, 897

Casey C. M. et al., 2009, MNRAS, 399, 121

Chapman S. C., Blain A. W., Smail I., Ivison R. J., 2005, ApJ, 622, 772

Chapman S. C., Blain A., Ibata R., Ivison R. J., Smail I., Morrison G., 2009, ApJ, 691, 560

Cox T. J., Di Matteo T., Hernquist L., Hopkins P. F., Robertson B., Springel V., 2006a, ApJ, 643, 692

Cox T. J., Dutta S. N., Di Matteo T., Hernquist L., Hopkins P. F., Robertson B., Springel V., 2006b, ApJ, 650, 791

Cox T. J., Jonsson P., Primack J. R., Somerville R. S., 2006c, MNRAS, 373, 1013

Cox T. J., Jonsson P., Somerville R. S., Primack J. R., Dekel A., 2008, MNRAS, 384, 386

D'Onghia E., Besla G., Cox T. J., Hernquist L., 2009, Nat, 460, 605

D'Onghia E., Vogelsberger M., Faucher-Giguere C.-A., Hernquist L., 2010, ApJ, 725, 353

Daddi E. et al., 2010, ApJ, 714, L118

Dasyra K. M. et al., 2006, ApJ, 638, 745

Dasyra K. M. et al., 2007, ApJ, 657, 102

Dasyra K. M., Yan L., Helou G., Surace J., Sajina A., Colbert J., 2008, ApJ, 680, 232

Dey A. et al., 2008, ApJ, 677, 943

Di Matteo T., Springel V., Hernquist L., 2005, Nat, 433, 604

di Matteo P., Combes F., Melchior A.-L., Semelin B., 2007, A&A, 468, 61

Dobbs C. L., Burkert A., Pringle J. E., 2011, MNRAS, 413, 528

Doyon R., Wells M., Wright G. S., Joseph R. D., Nadeau D., James P. A., 1994, ApJ, 437, L23

Evans N. J., II, 1999, ARA&A, 37, 311

Evans D. A. et al., 2010, ApJ, 710, 859

Evans N. J. et al., 2009, ApJS, 181, 321

Feruglio C., Maiolino R., Piconcelli E., Menci N., Aussel H., Lamastra A., Fiore F., 2010, A&A, 518, L155

Foster C., Proctor R. N., Forbes D. A., Spolaor M., Hopkins P. F., Brodie J. P., 2009, MNRAS, 400, 2135

Genzel R., Tacconi L. J., Rigopoulou D., Lutz D., Tecza M., 2001, ApJ, 563, 527

Genzel R. et al., 2010, MNRAS, 407, 2091

Governato F. et al., 2009, MNRAS, 398, 312

Governato F. et al., 2010, Nat, 463, 203

Guedes J., Callegari S., Madau P., Mayer L., 2011, ApJ, 742, 76

Hammer F., Flores H., Yang Y. B., Athanassoula E., Puech M., Rodrigues M., Peirani S., 2009a, A&A, 496, 381

Hammer F., Flores H., Puech M., Yang Y. B., Athanassoula E., Rodrigues M., Delgado R., 2009b, A&A, 507, 1313

Hayward C. C., Narayanan D., Jonsson P., Cox T. J., Kereš D., Hopkins P. F., Hernquist L., 2010, in Treyer M., Wyder T. K., Neill J. D., Seibert M., Lee Janice C., eds, ASP Conf. Ser. Vol. 440, UP2010: Have Observations Revealed a Variable Upper End of the Initial Mass Function? Astron. Soc. Pac., San Francisco, p. 369

Hayward C. C., Kereš D., Jonsson P., Narayanan D., Cox T. J., Hernquist L., 2011, ApJ, 743, 159

Hernquist L., 1989, Nat, 340, 687

Hernquist L., 1990, ApJ, 356, 359

Hernquist L., 1992, ApJ, 400, 460

Hernquist L., 1993, ApJ, 409, 548

Hernquist L., Barnes J. E., 1991, Nat, 354, 210

Hernquist L., Mihos J. C., 1995, ApJ, 448, 41

Hernquist L., Spergel D. N., Heyl J. S., 1993, ApJ, 416, 415

Hibbard J. E., Yun M. S., 1999, ApJ, 522, L93

Hoffman L., Cox T. J., Dutta S., Hernquist L., 2009, ApJ, 705, 920

Hoffman L., Cox T. J., Dutta S., Hernquist L., 2010, ApJ, 723, 818

Hopkins P. F., 2013, MNRAS, 428, 2840

Hopkins P. F., Hernquist L., 2009, ApJ, 694, 599

Hopkins P. F., Hernquist L., 2010, MNRAS, 402, 985

Hopkins P. F., Quataert E., 2010, ApJ, 407, 1529

Hopkins P. F., Quataert E., 2011a, MNRAS, 415, 1027

Hopkins P. F., Quataert E., 2011b, MNRAS, 411, L61

Hopkins P. F., Hernquist L., Martini P., Cox T. J., Robertson B., Di Matteo T., Springel V., 2005, ApJ, 625, L71

Hopkins P. F., Hernquist L., Cox T. J., Di Matteo T., Robertson B., Springel V., 2006, ApJS, 163, 1

Hopkins P. F., Cox T. J., Hernquist L., 2008a, ApJ, 689, 17

Hopkins P. F., Cox T. J., Kereš D., Hernquist L., 2008b, ApJS, 175, 390

Hopkins P. F., Hernquist L., Cox T. J., Dutta S. N., Rothberg B., 2008c, ApJ, 679, 156

Hopkins P. F., Hernquist L., Cox T. J., Kereš D., 2008d, ApJS, 175, 356

Hopkins P. F., Hernquist L., Cox T. J., Younger J. D., Besla G., 2008e, ApJ, 688, 757

Hopkins P. F., Cox T. J., Dutta S. N., Hernquist L., Kormendy J., Lauer T. R., 2009a, ApJS, 181, 135

Hopkins P. F., Cox T. J., Younger J. D., Hernquist L., 2009b, ApJ, 691, 1168

Hopkins P. F., Hernquist L., Cox T. J., Kereš D., Wuyts S., 2009c, ApJ, 691, 1424

Hopkins P. F., Lauer T. R., Cox T. J., Hernquist L., Kormendy J., 2009d, ApJS, 181, 486

Hopkins P. F. et al., 2009e, MNRAS, 397, 802

Hopkins P. F., Younger J. D., Hayward C. C., Narayanan D., Hernquist L., 2010, MNRAS, 402, 1693

Hopkins P. F., Quataert E., Murray N., 2011, MNRAS, 417, 950

Hopkins P. F., Quataert E., Murray N., 2012a, MNRAS, 421, 3488

Hopkins P. F., Quataert E., Murray N., 2012b, MNRAS, 421, 3522

Ivison R., Smail I., Papadopoulos P. P., Wold I., Richard J., Swinbank A. M., Kneib J., Owen F. N., 2009, MNRAS, 404, 198

James P., Bate C., Wells M., Wright G., Doyon R., 1999, MNRAS, 309, 585

Jesseit R., Cappellari M., Naab T., Emsellem E., Burkert A., 2009, MNRAS, 397, 1202

Jogee S. et al., 2009, ApJ, 697, 1971

Jonsson P., Cox T. J., Primack J. R., Somerville R. S., 2006, ApJ, 637, 255

Joseph R. D., Wright G. S., 1985, MNRAS, 214, 87

Juneau S., Narayanan D. T., Moustakas J., Shirley Y. L., Bussmann R. S., Kennicutt R. C., Jr, Vanden Bout P. A., 2009, ApJ, 707, 1217

Karl S. J., Naab T., Johansson P. H., Kotarba H., Boily C. M., Renaud F., Theis C., 2010, ApJ, 715, L88

Kennicutt R. C., Jr, 1998, ApJ, 498, 541

Kereš D., Vogelsberger M., Sijacki D., Springel V., Hernquist L., 2012, MNRAS, 425, 2027

Kewley L. J., Rupke D., Zahid H. J., Geller M. J., Barton E. J., 2010, ApJ, 721, L48

Khochfar S., Burkert A., 2006, A&A, 445, 403

Kitsionas S. et al., 2009, A&A, 508, 541

Kormendy J., Sanders D. B., 1992, ApJ, 390, L53

Kroupa P., 2002, Sci, 295, 82

Krumholz M. R., Gnedin N. Y., 2011, ApJ, 729, 36

Lake G., Dressler A., 1986, ApJ, 310, 605

Leitherer C. et al., 1999, ApJS, 123, 3

McGaugh S. S., 2005, ApJ, 632, 859

McKee C. F., Ostriker J. P., 1977, ApJ, 218, 148

Mac Low M.-M., Klessen R. S., 2004, Rev. Mod. Phys., 76, 125

Mannucci F., Della Valle M., Panagia N., 2006, MNRAS, 370, 773

Martin D. C. et al., 2007, ApJS, 173, 342

Melbourne J. et al., 2008, AJ, 136, 1110

Michard R., 2006, A&A, 449, 519

Mihos J. C., Hernquist L., 1994a, ApJ, 437, L47

Mihos J. C., Hernquist L., 1994b, ApJ, 431, L9

Mihos J. C., Hernquist L., 1996, ApJ, 464, 641

Moster B. P., Macciò A. V., Somerville R. S., Johansson P. H., Naab T., 2010, MNRAS, 403, 1009

Moster B. P., Macciò A. V., Somerville R. S., Naab T., Cox T. J., 2011, MNRAS, 415, 3750

Naab T., Burkert A., 2003, ApJ, 597, 893

Naab T., Burkert A., Hernquist L., 1999, ApJ, 523, L133

Narayanan D., Cox T. J., Hayward C., Younger J. D., Hernquist L., 2009, MNRAS, 400, 1919

Narayanan D., Hayward C. C., Cox T. J., Hernquist L., Jonsson P., Younger J. D., Groves B., 2010, MNRAS, 401, 1613

Narayanan D., Krumholz M., Ostriker E. C., Hernquist L., 2011, MNRAS, 418, 664

Narayanan D., Krumholz M. R., Ostriker E. C., Hernquist L., 2012, MNRAS, 421, 3127

Papovich C., Dickinson M., Giavalisco M., Conselice C. J., Ferguson H. C., 2005, ApJ, 631, 101

Pei Y. C., 1992, ApJ, 395, 130

Planesas P., Scoville N., Myers S. T., 1991, ApJ, 369, 364

Price D. J., Federrath C., 2010, MNRAS, 406, 1659

Puech M., Hammer F., Flores H., Neichel B., Yang Y., 2009, A&A, 493, 899

Purcell C. W., Kazantzidis S., Bullock J. S., 2009, ApJ, 694, L98

Rand R. J., Kulkarni S. R., 1990, ApJ, 349, L43

Reichardt C., Jimenez R., Heavens A. F., 2001, MNRAS, 327, 849

Robaina A. R. et al., 2009, ApJ, 704, 324

Robertson B. E., Bullock J. S., 2008, ApJ, 685, L27

Robertson B., Bullock J. S., Cox T. J., Di Matteo T., Hernquist L., Springel V., Yoshida N., 2006a, ApJ, 645, 986

Robertson B., Cox T. J., Hernquist L., Franx M., Hopkins P. F., Martini P., Springel V., 2006b, ApJ, 641, 21

Robertson B., Hernquist L., Cox T. J., Di Matteo T., Hopkins P. F., Martini P., Springel V., 2006c, ApJ, 641, 90

Rothberg B., Joseph R. D., 2004, AJ, 128, 2098

Rothberg B., Joseph R. D., 2006, AJ, 131, 185

Rupke D. S. N., Veilleux S., 2011, ApJ, 729, L27

Rupke D. S. N., Kewley L. J., Barnes J. E., 2010, ApJ, 710, L156

Saitoh T. R., Daisaka H., Kokubo E., Makino J., Okamoto T., Tomisaka K., Wada K., Yoshida N., 2008, PASJ, 60, 667

Saitoh T. R., Daisaka H., Kokubo E., Makino J., Okamoto T., Tomisaka K., Wada K., Yoshida N., 2009, PASJ, 61, 481

Sajina A., Yan L., Armus L., Choi P., Fadda D., Helou G., Spoon H., 2007, ApJ, 664, 713

Sánchez-Blázquez P., Forbes D. A., Strader J., Brodie J., Proctor R., 2007, MNRAS, 377, 759

Sanders D. B., Mirabel I. F., 1996, ARA&A, 34, 749

Sanders D. B., Soifer B. T., Elias J. H., Madore B. F., Matthews K., Neugebauer G., Scoville N. Z., 1988, ApJ, 325, 74

Sargent A. I., Sanders D. B., Scoville N. Z., Soifer B. T., 1987, ApJ, 312, L35

Schinnerer E. et al., 2008, ApJ, 689, L5

Scoville N. Z., Sanders D. B., Sargent A. I., Soifer B. T., Scott S. L., Lo K. Y., 1986, ApJ, 311, L47

Shier L. M., Fischer J., 1998, ApJ, 497, 163

Sijacki D., Vogelsberger M., Keres D., Springel V., Hernquist L., 2012, MNRAS, 424, 2999

Snyder G. F., Cox T. J., Hayward C. C., Hernquist L., Jonsson P., 2011, ApJ, 741, 77

Soto K. T., Martin C. L., 2010, ApJ, 716, 332

Springel V., 2005, MNRAS, 364, 1105

Springel V., 2010, MNRAS, 401, 791

Springel V., Hernquist L., 2002, MNRAS, 333, 649

Springel V., Hernquist L., 2003, MNRAS, 339, 289

Springel V., Hernquist L., 2005, ApJ, 622, L9

Springel V., Di Matteo T., Hernquist L., 2005, MNRAS, 361, 776

Stewart K. R., Bullock J. S., Wechsler R. H., Maller A. H., Zentner A. R., 2008, ApJ, 683, 597

Stewart K. R., Bullock J. S., Wechsler R. H., Maller A. H., 2009, ApJ, 702, 307

Sturm E. et al., 2011, ApJ, 733, L16

Swinbank A. M. et al., 2008, MNRAS, 391, 420

Tacconi L. J., Genzel R., Lutz D., Rigopoulou D., Baker A. J., Iserlohe C., Tecza M., 2002, ApJ, 580, 73

Tacconi L. J. et al., 2006, ApJ, 640, 228

Tacconi L. J. et al., 2008, ApJ, 680, 246

Tasker E. J., Tan J. C., 2009, ApJ, 700, 358

Teyssier R., Chapon D., Bournaud F., 2010, ApJ, 720, L149

Titus T. N., Spillar E. J., Johnson P., 1997, AJ, 114, 958

Torrey P., Cox T. J., Kewley L., Hernquist L., 2012a, ApJ, 746, 108

Torrey P., Vogelsberger M., Sijacki D., Springel V., Hernquist L., 2012b, MNRAS, 427, 2224

Tremonti C. A., Moustakas J., Diamond-Stanic A. M., 2007, ApJ, 663, L77

Vogelsberger M., Sijacki D., Keres D., Springel V., Hernquist L., 2012, MNRAS, 425, 3024

Walker I. R., Mihos J. C., Hernquist L., 1996, ApJ, 460, 121

Williams J. P., McKee C. F., 1997, ApJ, 476, 166

Wilson C. D., Scoville N., Madden S. C., Charmandaris V., 2003, ApJ, 599, 1049

Wilson C. D., Harris W. E., Longden R., Scoville N. Z., 2006, ApJ, 641, 763

Wuyts S. et al., 2009, ApJ, 700, 799

Wuyts S., Cox T. J., Hayward C. C., Franx M., Hernquist L., Hopkins P. F., Jonsson P., van Dokkum P. G., 2010, ApJ, 722, 1666

Yan L., Sajina A., Fadda D., Choi P., Armus L., Helou G., Teplitz H., Frayer D., Surace J., 2007, ApJ, 658, 778

Yang Y., Hammer F., Flores H., Puech M., Rodrigues M., 2009, A&A, 501, 437

Younger J. D. et al., 2007, ApJ, 671, 1531

Younger J. D., Hopkins P. F., Cox T. J., Hernquist L., 2008a, ApJ, 686, 815

Younger J. D. et al., 2008b, ApJ, 688, 59

Younger J. D., Hayward C. C., Narayanan D., Cox T. J., Hernquist L., Jonsson P., 2009a, MNRAS, 396, L66

Younger J. D. et al., 2009b, ApJ, 704, 803

Zuckerman B., Evans N. J., II, 1974, ApJ, 192, L149

APPENDIX A: SIMULATION IMAGES

Figs A1–A8 present the images of the rest of our simulations, at different viewing angles and times during the mergers, in the style of Figs 1 and 2. Movies and additional images are available online (https://www.cfa.harvard.edu/~phopkins/Site/Movies_sbw_mgr.html).
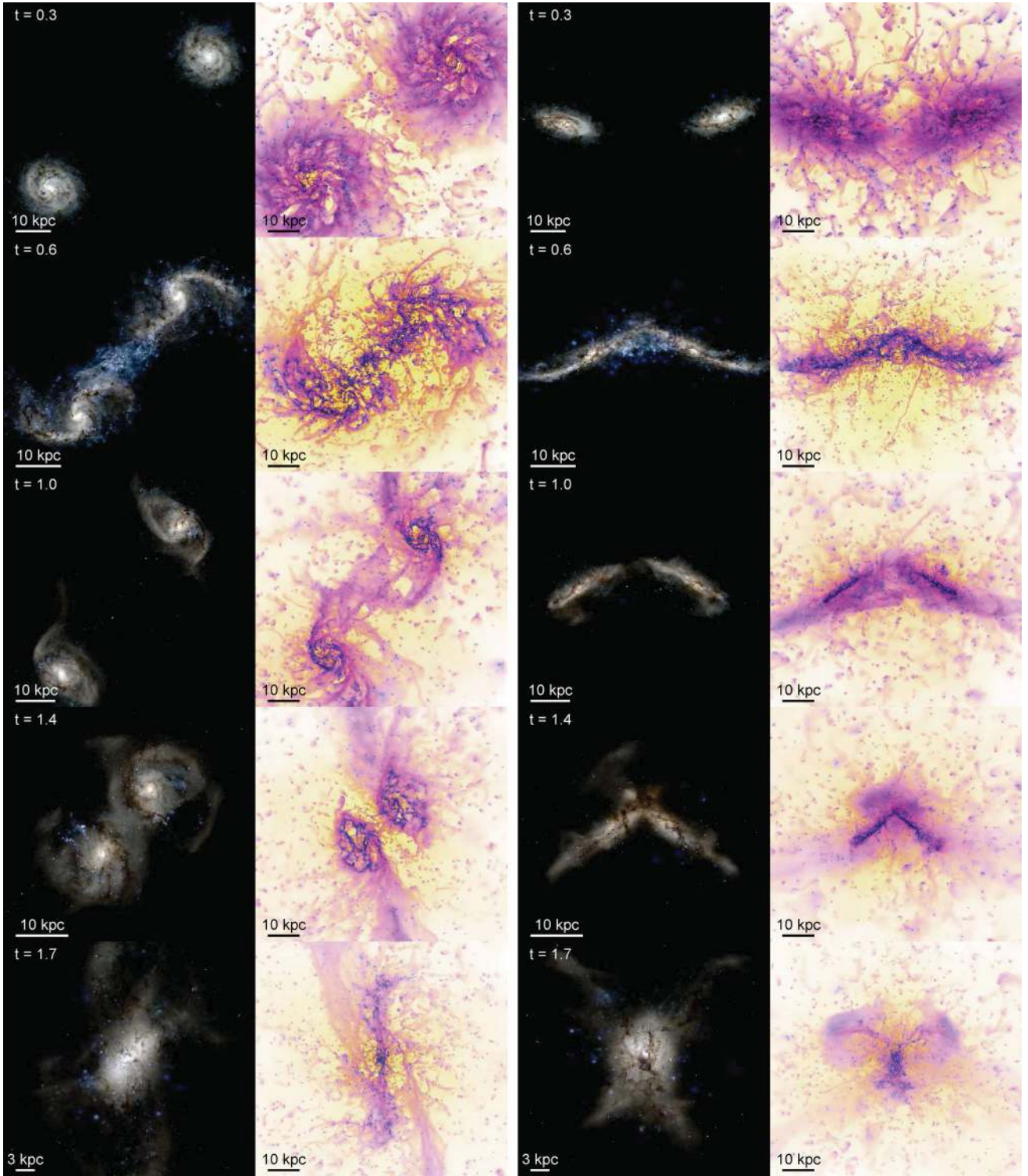
Figure A1. Morphology of the *e* (prograde) merger of the Sbc galaxy (a dwarf starburst). We show two perpendicular viewing angles (left-hand and right-hand panels); each shows the optical (as Fig. 2; left-hand panels) and gas (as Fig. 1; right-hand panels). The time since the start of the simulation (in Gyr) is labelled. From the top to bottom, the merger stages are: (1) pre-merger infall, (2) just after the first passage, (3) apocentre/turnaround, (4) final merger and (5) just after nuclear coalescence.
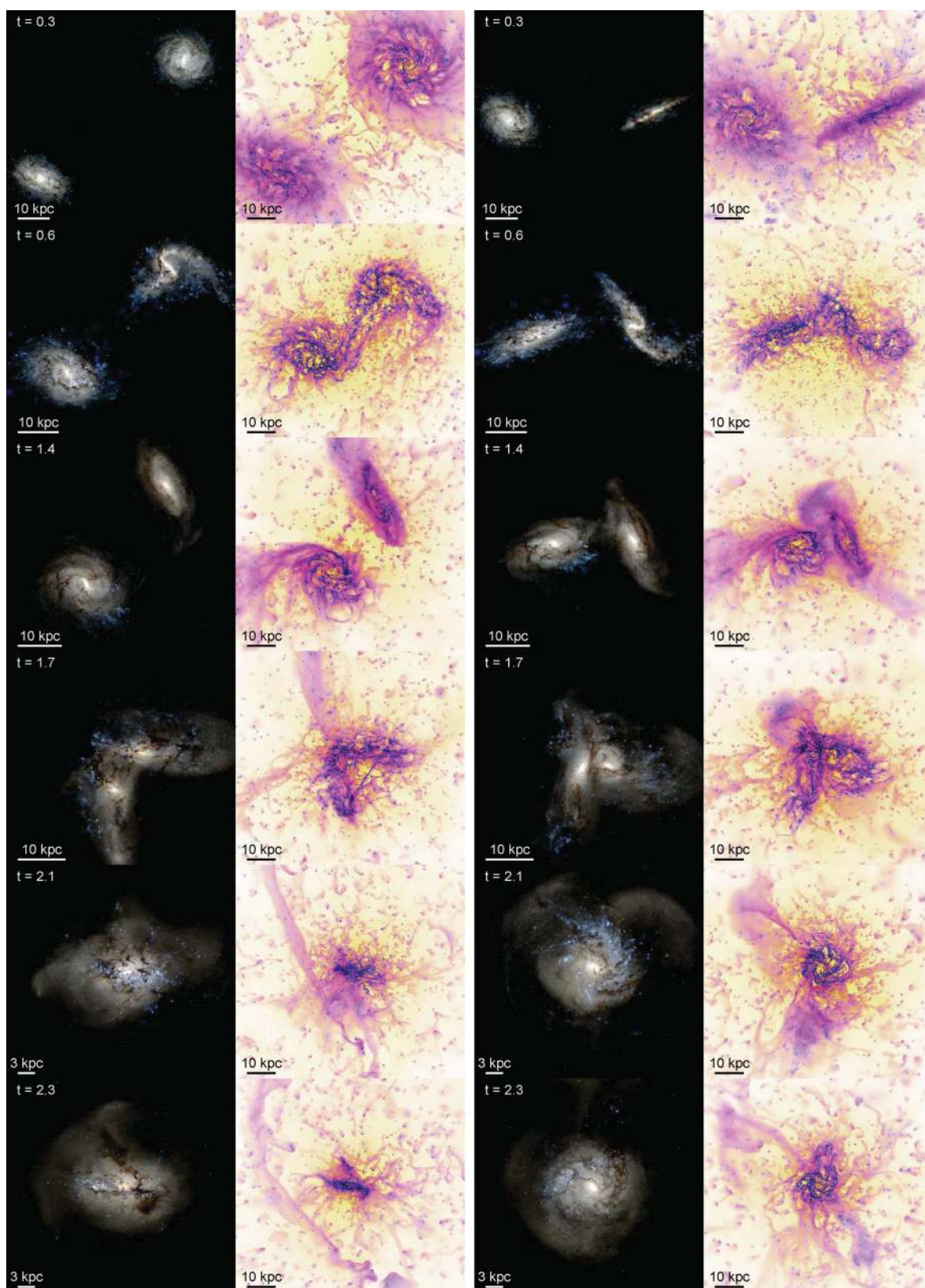
Figure A2. As Fig. A1, for the *f* (retrograde) Sbc merger.
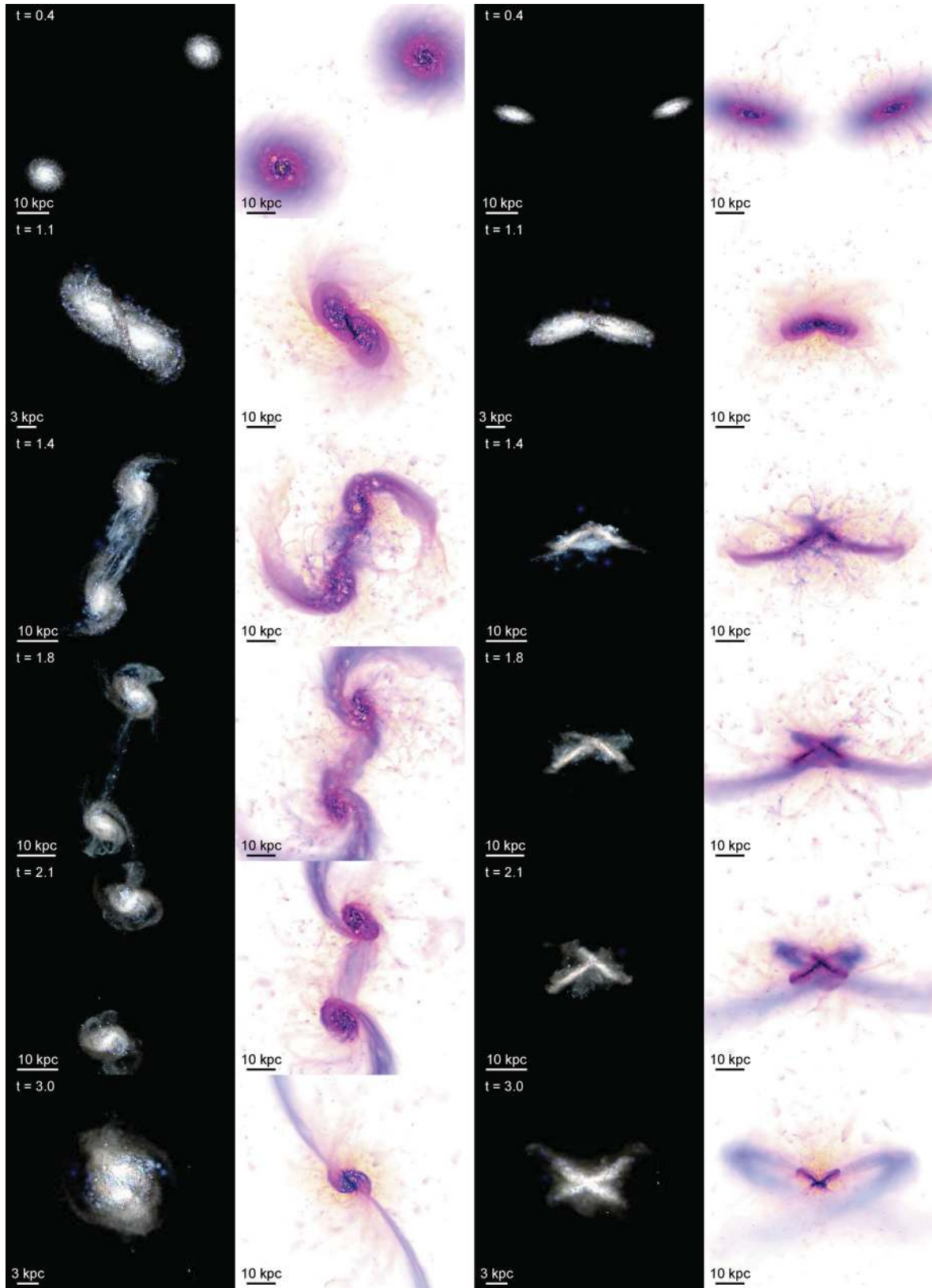
Figure A3. As Fig. A1, for the SMC (SMC–mass dwarf) *e* merger.
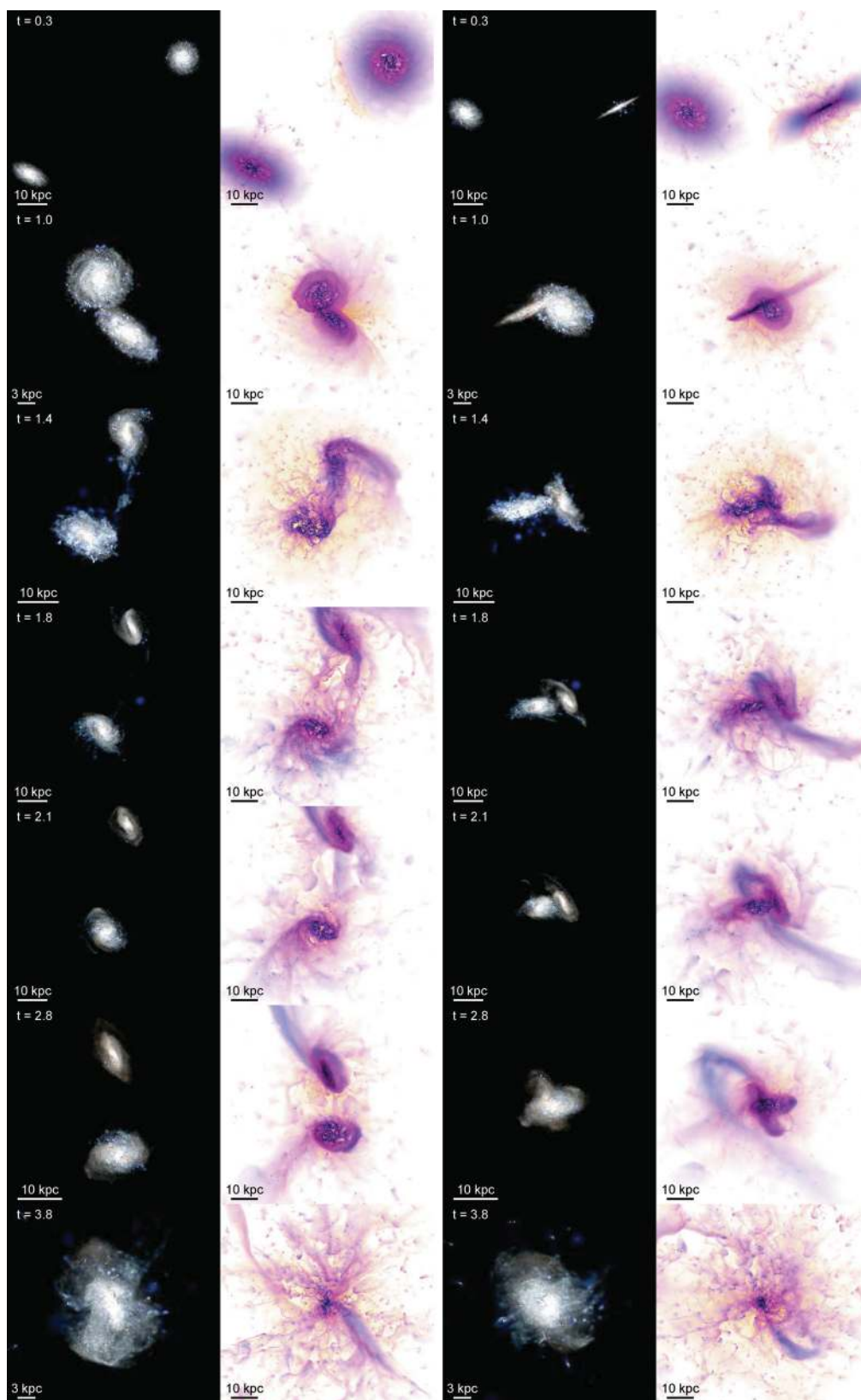
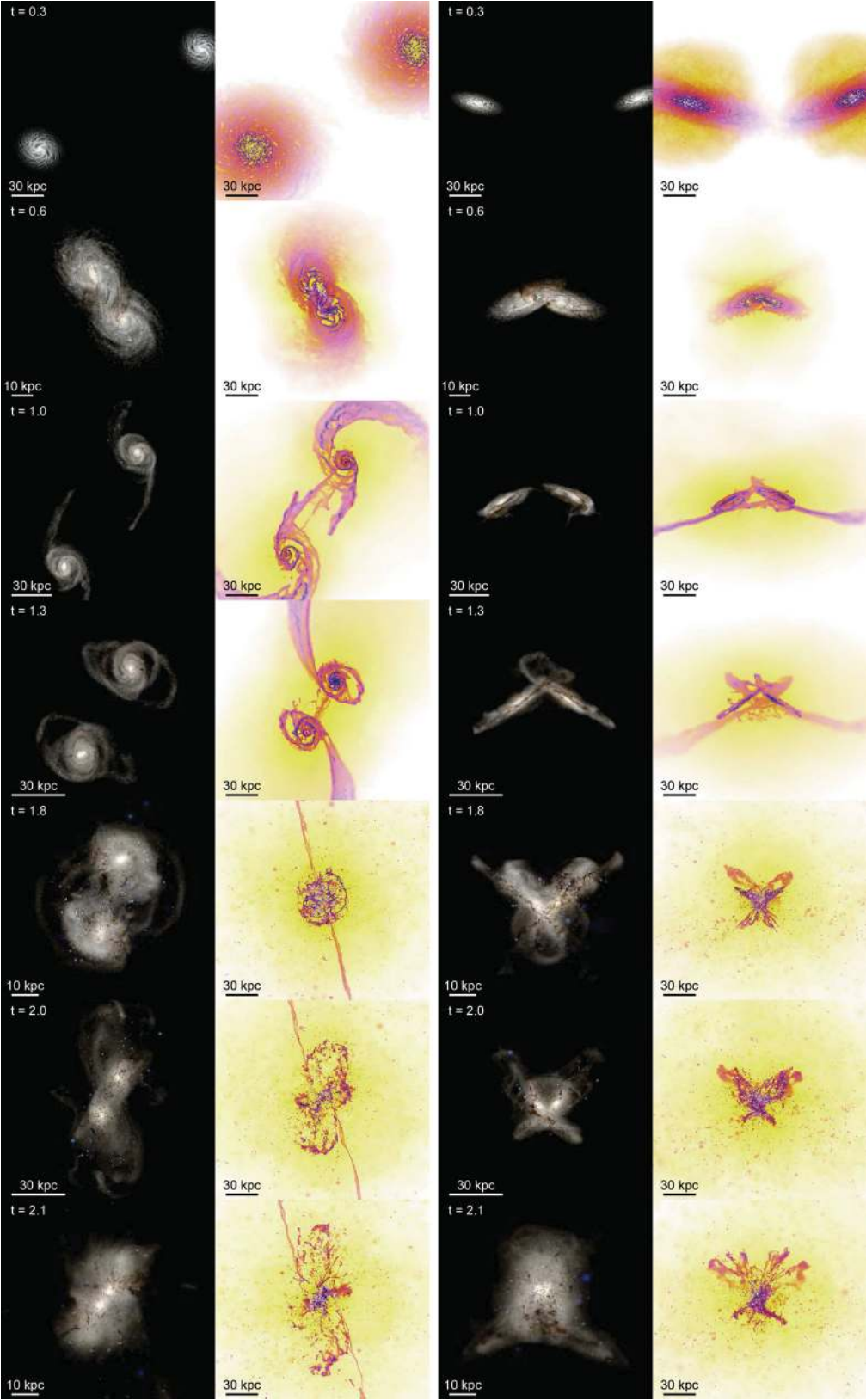**Figure A4.** As Fig. A1, for the SMC f merger.

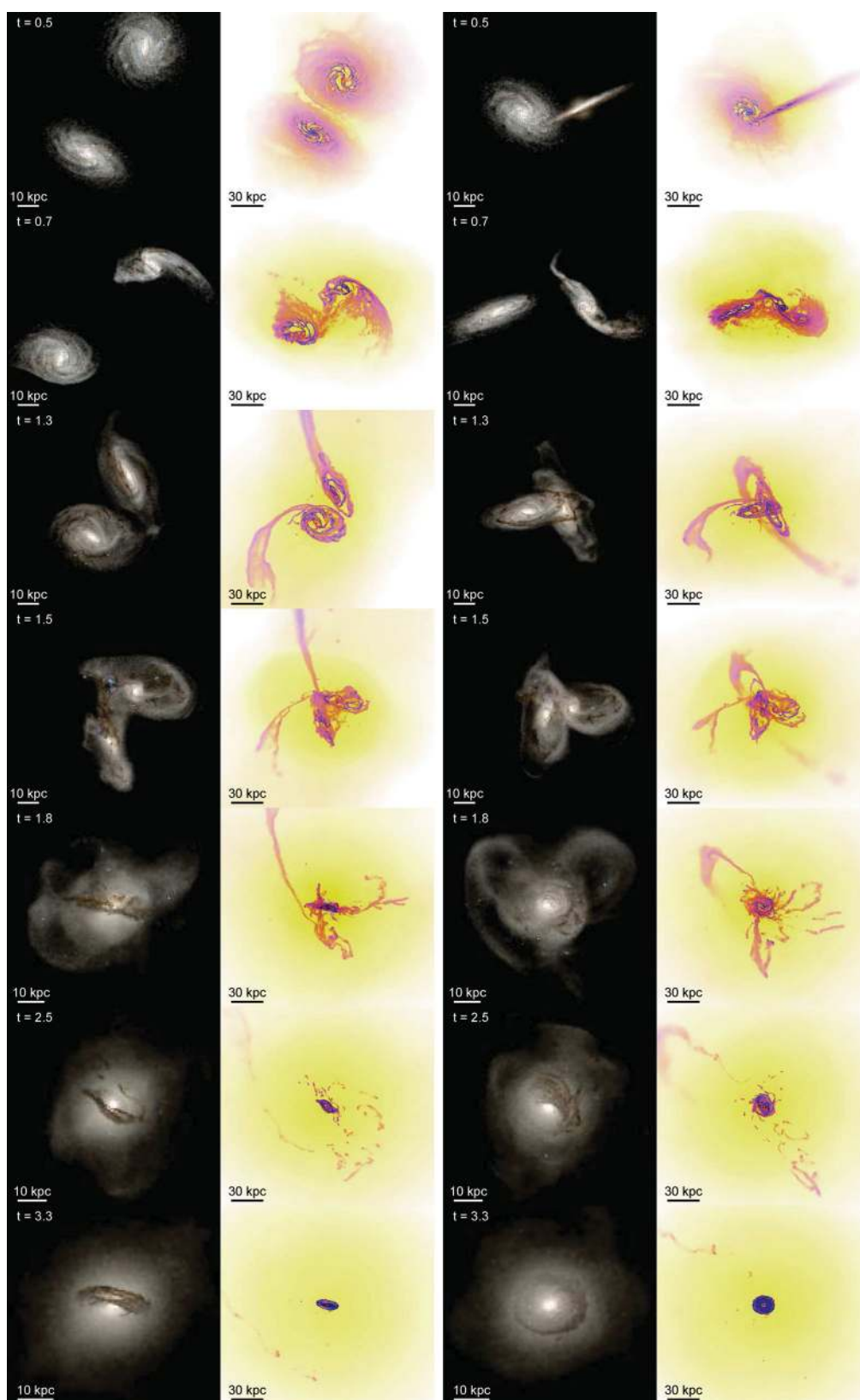**Figure A5.** As Fig. A1, for the MW *e* merger.

Figure A6. As Fig. A1, for the MW *f* merger.

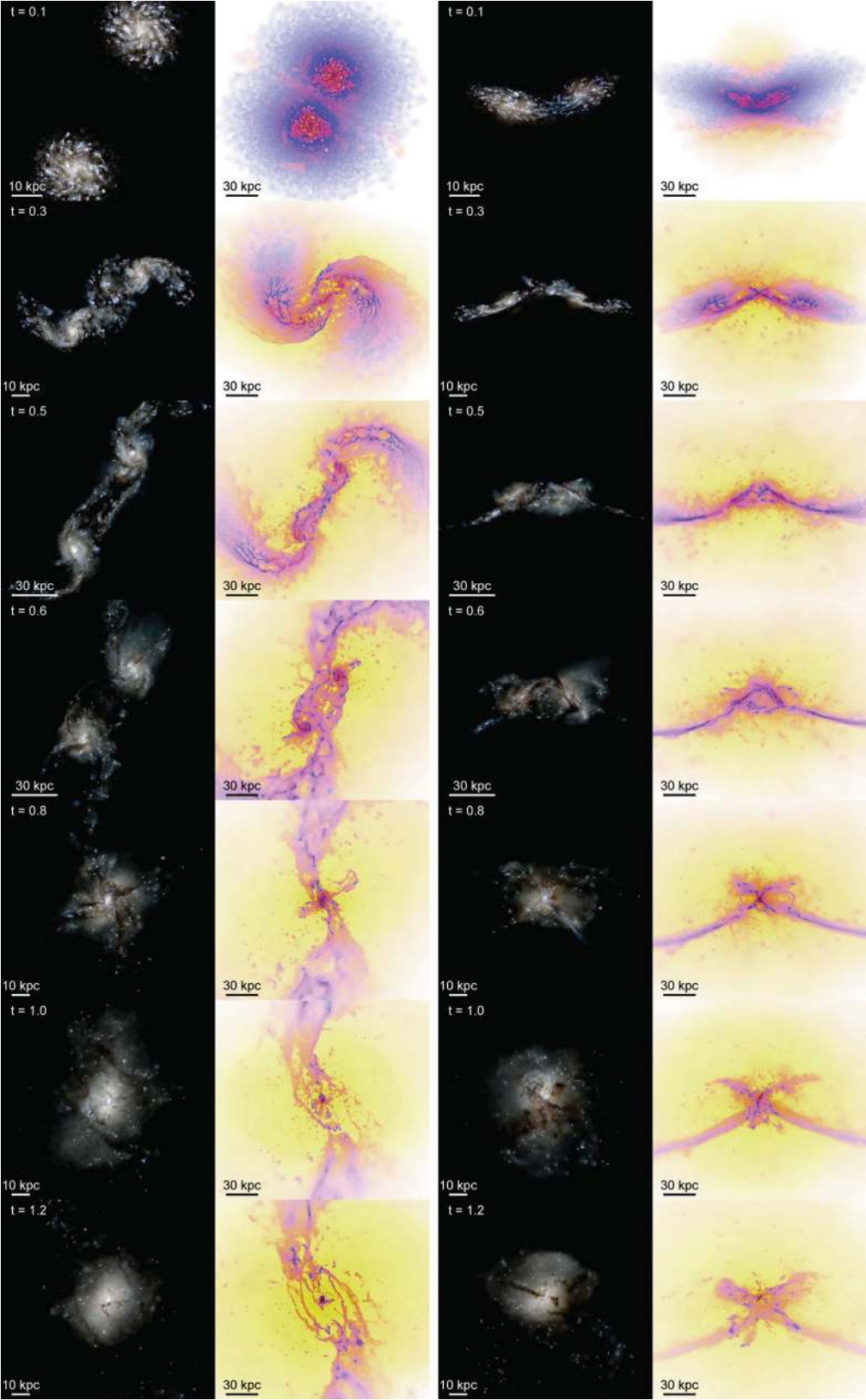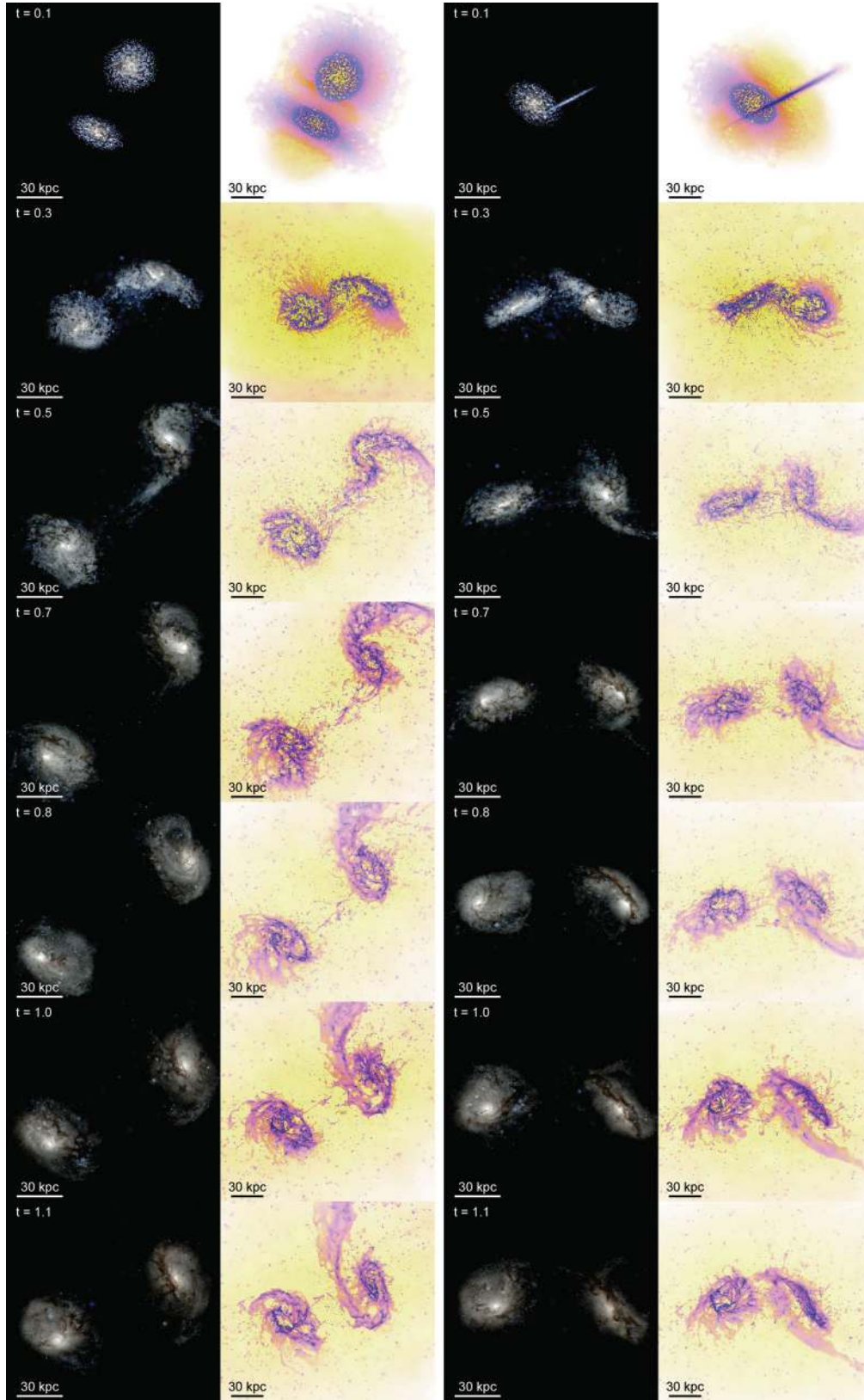**Figure A7.** As Fig. A1, for the HiZ *e* merger.

Figure A8. As Fig. A1, for the HiZ f merger.

This paper has been typeset from a TEX/LATEX file prepared by the author.